Harvesting Wind Energy via the Triboelectric Effect

A Technical Report submitted to the Department of Mechanical and Aerospace Engineering

Presented to the Faculty of the School of Engineering and Applied Science

University of Virginia • Charlottesville, Virginia

In Partial Fulfillment of the Requirements for the Degree

Bachelor of Science, School of Engineering

Spring, 2025

Essam Allibhai-Mawani
Anthony Ferrufino Cruz
Christopher Herath
Grace Hessberg
Steve Kim
Oliver Nicholson
Graham Osisek
Sage Wibberley

On our honor as University students, we have neither given nor received unauthorized aid on this assignment as defined by the Honor Guidelines for Thesis-Related Assignments

Technical Advisors:

Sarah Sun and Thomas Ward, Department of Mechanical and Aerospace Engineering

Table of Contents

Executive Summary

Transitioning the energy sources used globally from traditional thermal or fossil fuels to renewables is one way to tackle climate change and decrease the greenhouse gases emitted. Although wind and solar renewable energy systems are well developed, there is a need for small-scale options for wind energy systems, particularly in densely populated areas. Currently, small wind turbines are not efficient due to limited energy output, inconsistent wind patterns in urban areas, and a relatively high cost. By developing an array of bio-inspired "leaf" structures that utilize the triboelectric effect to generate electricity, this project aims to add a component to the energy transition within distributed wind technologies.

Our team worked to identify triboelectric materials to use for this project, of which we picked teflon and copper. We developed cylindrical and flat blades that informed and led to our final design of a "leaf". Throughout prototyping, we used a flexible 3D printed plastic, Thermoplastic Polyurethane (TPU), to rapidly prototype and test a variety of different shapes. Repeated contact and separation of the two tribal materials creates voltages peaks, similar to alternating current (AC). This AC voltage is converted to a smoother, almost direct current (DC) like voltage output through the electrical system consisting of a bridge rectifier and a capacitor.

Problem Statement

In July 2018, a record-breaking heatwave hit Japan (Merino, 2020). Over 10,000 people were hospitalized and 1,000 people were killed from the heat (Merino, 2020). Climate scientists later found that this natural catastrophe would be completely impossible if it were not for climate change (Merino, 2020). Climate change can be best defined as "long-term shifts in temperatures and weather patterns" (United Nations [UN], n.d.-a). While these noticeable shifts can be a natural result of the environment, the recent shifts are primarily caused by greenhouse gas

(GHG) emissions from human activities, especially the burning of fossil fuels. Burning fossil fuels like oil, coal, and gas results in the release of GHGs like carbon dioxide and methane into the atmosphere. After being released into the atmosphere, these chemicals trap more heat irradiated from the sun and raise the planet's average temperature (UN, n.d.-a). In 2023, fossil fuels made up 84% of the United States' primary energy production (Energy Information Administration [EIA], 2024). Fossil fuel burning must be dramatically reduced in the U.S. to avoid future disasters that make thousands into casualties of climate change.

One of the alternatives to fossil fuel is renewable energy generated by wind turbines. Renewable energy is "energy derived from natural sources that are replenished at a higher rate than they are consumed," (UN, n.d.-b). Wind turbines are one of the most cost effective forms of energy generation and work well in rural or mixed-used areas (The Office of Energy Efficiency and Renewable Energy [EERE], n.d.). But, wind turbines' need for high wind speeds often pushes them into remote areas far from cities where energy the most (EERE, n.d.). Even if there was high enough wind in a city, wind turbines tend to be noisy and alter visual aesthetics which most people don't appreciate (EERE, n.d.).

Wind energy generation must be accessible to cities throughout the United States to combat the climate crisis. In pursuit of this goal, our team set out to create a new form of wind generation that could utilize the low wind speeds found in cities without the disruption brought by conventional wind turbines.

Research & Literature Review

Throughout the U.S., renewable energy generation has been increasing, accounting for around 21% of the total kilowatt hours (kWh) of electricity produced in 2023 (*What Is U.S. Electricity Generation by Energy Source?*, n.d.). Wind energy made up the largest portion of

renewable energy at around 10% of the total amount of electricity produced in the U.S. (*What Is U.S. Electricity Generation by Energy Source?*, n.d.). However, wind energy turbines, the most common method for harvesting wind energy, are only efficient in open areas with consistent high wind speeds like agricultural lands and coastal or island communities (*Advantages and Challenges of Wind Energy*, n.d.). This has led to typical renewable energy generation requiring "at least 10 times as much land per unit of power produced than coal or natural gas fired power plants, including land disturbed to produce and transport the fossil fuels" (Gross, 2020). In addition, wind turbines have a cut-in speed and below which they do not generate electricity, typically between 6 and 9 mph (Office of Energy Efficiency & Renewable Energy, 2024). For a state like Virginia where most regions have average wind speeds less than 4 m/s (9 mph), large wind turbines are not viable in urban areas and areas with low or inconsistent wind speeds (AWS Truepower & National Renewable Energy Laboratory, NREL, n.d.). Therefore, it is difficult to integrate large wind turbine structures into highly populated urban areas due to an apparent lack of space and low and/or irregular wind speeds.

One solution for urban wind generation already in practice is to use building-integrated wind energy from smaller wind turbines that are integrated into the top of buildings along the "building parapets" (Wilson, 2009). Building parapets are areas at the top of the building where the wind rises up and curls over the edge creating a higher wind velocity (Wilson, 2009). Some architects have even developed funnels along these edges to channel the wind at higher speeds to increase efficiency of the building-integrated wind turbines (Wilson, 2009). Although these integrated wind turbines allow urban areas to utilize the wind, they are less efficient than standard wind turbines (Wilson, 2009). Another issue is the noise and vibrations it causes to the

building. Just isolating it takes up an entire floor of the building, and the frequency must match the HVAC systems to prevent the entire building from shaking (Wilson, 2009).

Other innovative technologies such as piezoelectronics have been created for compact energy-harvesting on a small scale. The high cost and rarity of piezoelectric materials creates a hindrance for their wide scale adoption. A new solution to this problem is to combine compact energy harvesting with wind energy by utilizing the triboelectric effect, better known as static electricity, because it can make use of many common materials, thereby being less expensive and more available. The theory surrounding triboelectricity is somewhat sparse and continuously being developed, but some basic models exist to describe its operation. Leading theory states that the phenomenon occurs when two materials with opposite triboelectric properties come into contact, causing electrons to transfer from the positive material to the negative. Although triboelectricity has been acknowledged for over 2000 years, many basics remain poorly understood (*Triboelectricity*, n.d.). Triboelectricity is a field that is gaining more interest; while in 2012 there were only 8 articles published on TENGS, in 2018 that number increased to 444 (Cheng et al., 2019). Some underdeveloped topics of research include how charge is transferred and what determines the triboelectric charge of a material (Lacks & Shinbrot, 2019). One generally accepted theory for solid-solid triboelectrification (as opposed to solid-liquid) proposes that as two atoms or molecules come into close enough proximity, their electron clouds 'overlap', allowing for the electron to tunnel between the two materials (Xu et al., 2018). When one connects the negative and positively charged materials, they act similarly to the terminals of a battery, supplying a brief current of electricity that can be collected and used like any other source of electricity.

Ideation

Early steps were taken to ensure the effective development of a triboelectric wind generator. Actions performed prior to the analysis and design process included: an ideation process in which team members workshopped various designs, a selection and screening process that sorted the best ideas, development of specifications to assess success of later designs, testing of various materials being considered, cementing/further development of design specifications, and development of a rectifier circuit used to manage data collection. These early tasks provided groundwork for focussed progress later in the project's development, and enabled approach to the design phase with clear objectives and goals.

The design process began with each member of the group developing several concepts that could serve in a system to create triboelectricity. This approach encouraged each member to brainstorm diverse ideas. From there, the group reconvened and performed a first round of screening to select the most reasonable ideas to further pursue. This screening was performed on a total of 24 different ideas, with 6 of them being scored the highest and thus screened in a second round. The 6 that proceeded to a further round of screening are concepts A, J, B, V, D, and O that are seen in Figures 1-6. In addition, concepts TK and AV (Figures 7 and 8) were developed by combining multiple ideas to create an optimal, hybrid design.

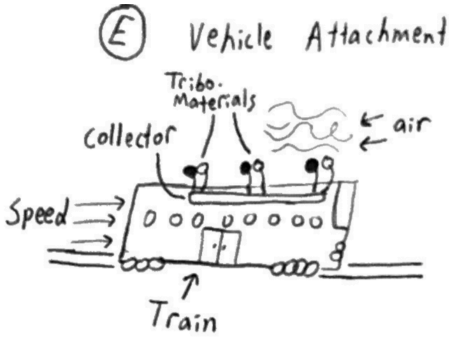

Figure 1: Concept A

Figure 2: Concept J

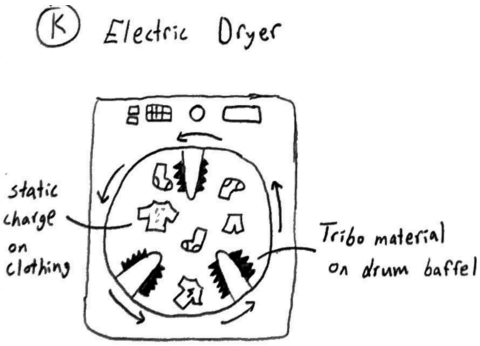

Figure 3: Concept B

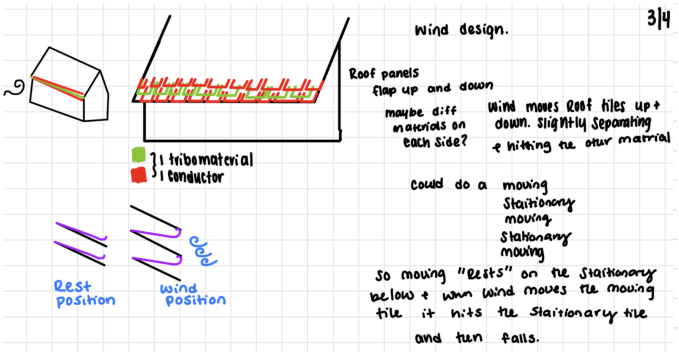

Figure 4: Concept D

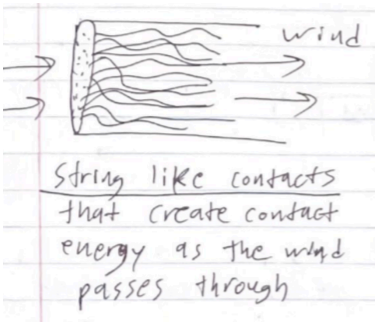

Figure 5: Concept V

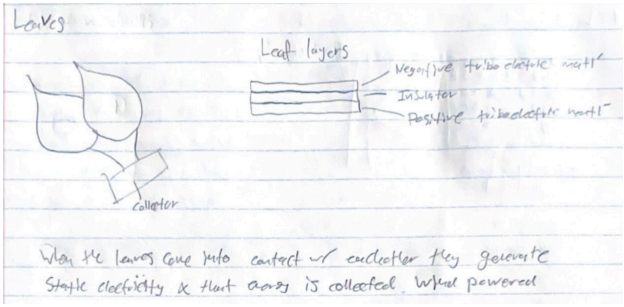

Figure 6: Concept O

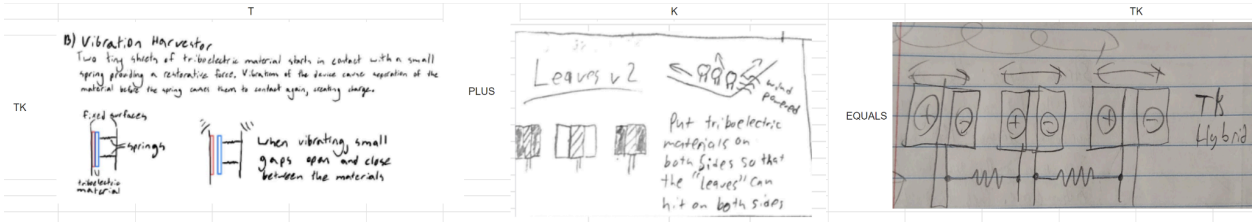

Figure 7: Hybrid concept TK

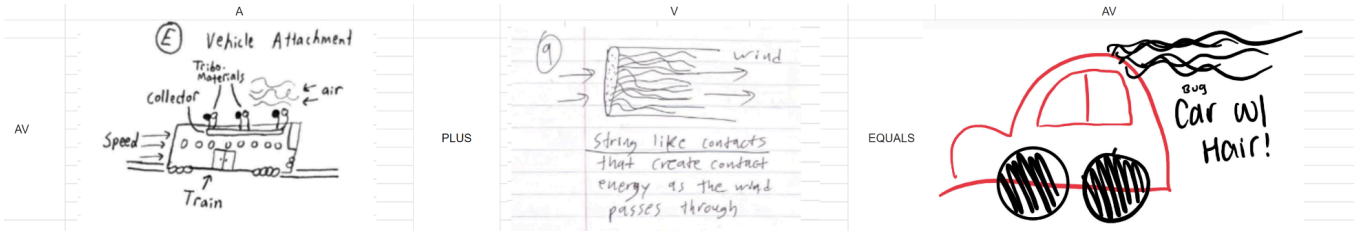

Figure 8: Hybrid concept AV

Selection and Screening

Each team member selected three of their own design ideas for initial screening. These 24 concepts were screened and ranked on 10 selection criteria as shown in Figure 9. Then, the top six designs, along with two hybrid designs, moved on to concept scoring, shown in Figure 10. Power generation is the highest weighted criteria because it is the primary purpose of the device and directly determines the product's value. Ease of installation, ease of access/repair, and scalability were important design considerations that deserved increased weight. Using our initial specifications in tables 2, 3, and 4 further below, each design was ranked out of five points and summed up. Concept J in Figure 2 was selected as the design to pursue.

			Counting: All members present														
	Each Person Picked 3 of their Ideas		Benchmark: Leaf idea presented by professors (tribo)														
	0 = the same as the leaf idea, +1 = better than the leaf idea, -1 = worse than the leaf idea																
			Concept Variants														
			Essam	Chris	Essam	Grace	Steve	Graham	Chris	Anthony	Anthony	Oliver	Graham	Grace	Graham	Sage	Sage
Selection Criteria	Descriptions	LEAF	Idea A	Idea A	Idea B	Idea A	Idea A	Idea C*	Idea B*	Idea A"	Idea B	Idea A	Idea A	Idea B"	Idea B	Idea A`	Idea B
			A	J	B	D	V	O	K	P	Q	G	M	E	N	S	T
Power generated	Hypothesized power/area	0	6	2	0	1	2	2	2	2	-4	-2	4	1	-3	-4	0
Life span	life span	0	2	2	-4	5	0	-2	-1	0	0	1	0	0	-2	-1	-2
Maintenance	how often needs repair	0	-2	-1	0	3	0	0	-2	-3	-1	0	-2	0	-1	-1	0
Aesthetics	Will people think it looks good	0	-1	4	3	0	1	0	0	0	5	1	2	0	0	1	3
Weight	Will it be too heavy for the surface it's applied on	0	5	0	4	5	5	0	0	0	3	1	1	0	0	0	0
Qualification 6	How many products can be applied to a surface while it's still harvesting energy	0	5	5	0	0	3	2	1	-1	-6	-3	4	-2	0	-2	-4
Ease of access/repair	how hard is it to repair	0	3	2	5	-3	3	0	0	1	3	-3	-4	0	0	1	-3
Ease of installation	time/effort required to install	0	2	4	4	0	3	1	0	2	3	0	-4	0	1	-1	1
Environmental resistance	Resistance to all weather conditions	0	0	1	4	3	-4	-2	0	0	-4	3	-3	-2	-1	6	3
Safety	Dangerous to operate	0	2	0	1	0	0	0	0	-1	1	0	0	0	3	-2	-1
Sum		**0**	**22**	**19**	**17**	**14**	**13**	**1**	**0**	**0**	**0**	**-2**	**-2**	**-3**	**-3**	**-3**	**-3**
Rank		N/A	1	2	3	4	5	6	7	7	7	8	8	9	9	9	9
Continue?		N/A															

Figure 9: Selection Criteria Screening Sheet.

We choose idea J

We compared to the leaf idea. same as leaf = 3. better 4 or 5 and worse 1 or 2, based on our criteria

We each selected 3 ideas and ranked them in the selection criteria sheet on this file. and then ranked the top 6. this sheet is ranking the top 6 ideas

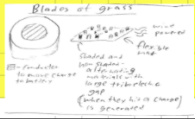

< idea J

			Reference: Professor Leaf		A								J									B								
Selection Criteria	Descriptions	Weight	Rating	Weighted Score	1	2	3	4	5	6	7	8	avg	Weighted Score	1	2	3	4	5	6	7	8	avg	Weighted Score	Rating	1	2	3	4	5	6	7	8	avg	Weighted Score
Power generated	Hypothesized power/area	18		0	3	3	3	3	2	2	3	2.8	9.9	2	4	3	4	3	2	4	4	3.3	11.7		3	3	4	2	3	1	1	2	2.4	8.6
Life span	life span	8		0	2	3	3	3	2	3	3	3	2.8	4.4	3	3	3	4	2	3	2	4	3.0	4.8		2	2	3	3	2	3	4	1	2.5	4.0
Maintenance	how often needs repair	10		0	2	2	3	3	3	3	2	3	2.6	5.3	3	3	2	4	2	4	3	4	3.1	6.3		2	2	2	2	2	2	3	2	2.1	4.3
Aesthetics	Will people think it looks good	2		0	2	4	4	3	3	2	4	4	3.3	1.3	3	4	2	3	3	3	3	4	3.1	1.3		4	4	3	3	4	5	3	3	3.6	1.5
Weight	Will it be too heavy for the surface it's applied on	8		0	3	3	4	4	4	4	3	4	3.6	5.8	2	3	4	3	4	2	5	4	3.4	5.4		4	3	3	3	3	5	3	4	3.5	5.6
Qualification 6	How many products can be applied to a surface while it's still harvesting energy	12		0	3	4	4	4	3	4	4	2	3.5	8.4	4	5	5	4	4	4	5	4	4.4	10.5		1	1	2	1	2	1	1	3	1.5	3.6
Ease of access/repair	how hard is it to repair	12		0	3	4	4	2	3	3	3	3	3.1	7.5	3	3	3	3	2	2	2	3	2.6	6.3		2	4	3	2	2	4	2	4	2.9	6.9
Ease of installation	time/effort required to install	12		0	2	4	2	2	3	4	2	3	2.8	6.6	3	3	3	3	3	3	3	3	3.0	7.2		3	4	2	2	2	4	2	4	2.9	6.9
Environmental resistance	Resistance to all weather conditions	10		0	3	2	2	3	2	3	1	3	2.4	4.8	3	4	3	3	2	1	3	3	2.8	5.5		4	2	4	3	3	3	4	3	3.3	6.5
Safety	Dangerous to operate	8		0	1	1	4	3	4	4	3	4	3.0	4.8	4	4	4	3	4		4	4	3.9	6.2		3	2	4	3	4	3	3	4	3.3	5.2
	Total Score	100		0										58.7										65.1										53.0
	Rank	N/A												4										1										8
	Winner	N/A																						YES										

Figure 10: Concept Scoring Sheet

Initial Specifications and Prototypes

The triboelectric wind energy harvester specifications are split into three main categories: function, design, and environmental impact. These categories set the foundation for how the device performs, how user-friendly it is, and how it impacts the environment. Functional specifications cover important metrics such as power generation, lifespan, and cost, ensuring the harvester can meet energy production targets effectively. Design specifications focus on practical aspects, such as making the device modular, easy to install, and adaptable to different wind speeds and roof placement. Environmental specifications ensure the device is durable, safe, and eco-friendly so it can handle various weather conditions while minimizing environmental harm. By turning these initial ideas into clear, measurable goals, the project aims to create a product that works well in the real world and meets its technical and sustainability objectives.

Table 1

Functional Specifications (Initial Specifications)

#	Specification	Measurement/Units
1	Power Generated	Power, Voltage, Amperage per Area or Volume
2	Amperage Generated	Amperage/Area or Volume
3	Harnesses energy from the environment	Yes or no- is power generated
4	Sustained power generation	Power vs time graph
5	Life Span	Number of cycles it withstands
6	Cost	Cost
7	Maintenance	# of times need to be maintenance in certain time frame
8	Transportability	Durability Testing (if fragile or not) Need special transport? Weight & Size
9	Aesthetics	Survey
10	Weight	Weight

Table 2
Design Specifications (Initial Specifications)

#	Specification	Measurement/Units
11	Size	Area
12	Output energy format	AC or DC
13	Optimal Wind speed	Compare power generated at different wind speeds
14	Triboelectric gap in Materials used	Peak voltage/difference in determined triboelectric series
15	Ease of Access/Repair	Survey, number of steps and number of parts
16	Ease of Installation	Survey, number of parts, number of steps, and average time to install
17	Modular	# of components Able to be easily put together? (Y/N)
18	Complexity of manufacture	Cost Number of components scalable/rarity of materials

Table 3

Environmental Specifications (Initial Specifications)

#	Specification	Measurement/Units
19	Environmental Resistance	Durability testing results in different environmental conditions
20	Environmentally conscious	Materials used: Rarity, toxicity, etc. Design for end of life: % of material that can be easily repurposed, etc.
21	Safety	Number and ranked severity of potential hazards

Material Testing

Background

The purpose of material testing was to determine the best possible combination of weather-resistant, off-the-shelf materials that generate the largest charge. This charge is generated when two triboelectrically dissimilar materials come into contact, with the "positive" material tending to lose electrons to the "negative" material which tends to gain them, based on the material's electron affinity (Wu et al., 2019). A conductive material can be placed between the two surfaces to collect and transmit the generated charge (Xu et al., 2018). The higher the voltage and current that can be generated, the greater the power that is available to be reused. This relationship can be quantified by the power equation shown below.

$$P = \frac{1}{2}(V_0 I_0) \text{ (Watts)} \quad (1)$$

In equation (1), P is electric power, V_0 is peak voltage, and I_0 is peak current. An alternating current is created by contact separation, resulting in voltage spikes as illustrated in Figure 11 below (Zou et al., 2019).

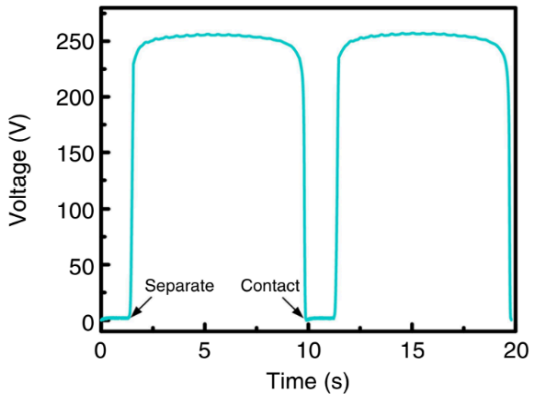

Figure 11: Typical output of open-circuit voltage for two cycles of contact separation (Zou et al., 2019)

By identifying the material pairings that generate the highest spikes in voltage, this testing informed the selection of optimal pairs of triboelectric materials to maximize voltage in the final system design. Additionally, the materials need to be thin enough to reduce the internal resistance and to allow for ease of application.

Force to Voltage Calculations

To determine the amount of voltage that can be generated from the contact separation method of triboelectric generation between different materials, the theoretical triboelectric surface-charge-distance equation as shown in equation (2) below, can be used. V is the voltage, Q is the total transferred charge, A is the contact surface area, d_{Foam} represents the thickness of the materials, ε_{Foam} represents the material dielectric constant, ε_0 is the vacuum dielectric constant of the space between the materials, σ is the surface charge density, and x(t) is the distance of separation of the materials between contacts.

$$V = -\frac{Q}{A\epsilon_0}\left[\frac{d_{Foam}}{\epsilon_{Foam}} + x(t)\right] + \frac{\sigma x(t)}{\epsilon_0}\ (\text{Volts}) \qquad (2)$$

Based on equation (2), increasing contact separation distance increases impact force, which results in a higher voltage due to a larger transferred charge. It is assumed that there is a perfect contact and charge transfer where $Q=Q_0$, and $Q=\sigma*A$. Distance and force will have minimal impact on the voltage outputs due to these assumptions. A constant separation distance of 0.154 m and material thicknesses of 0.0015 m are also assumed.

Table 4

Properties of single material

Assuming Q=Q_0	Teflon	PVC	Silicon rubber
Charge density (C)	1.13E-04	1.18E-04	7.00E-05
Thickness (m)	0.0015	0.0015	0.0015
Dielectric constant	2.1	4	3.2
Vacuum Dielectric constant	8.86E-12	8.86E-12	8.86E-12
Final Voltage (V)	9.12E+03	4.97E+03	3.70E+03

Table 4 shows the pertinent material properties used in calculating the theoretical voltage that is generated from contact separation of just the negatively charged materials. Teflon has a dielectric constant of 2.1 and the largest expected voltage of 912 Volts. The lower the dielectric constant is, the higher the voltage the material can handle before breaking down, resulting in a larger voltage output.

Table 5

Electrical Properties and Resulting voltages with Teflon Paired with Various Positive Triboelectric materials

Assuming Q=Q_0	Teflon With Cellulose	Teflon With Nylon	Teflon With Foam
Charge density (Coulombs)	3.33E-05	8.50E-05	1.36E-04
Thickness (m)	0.0015	0.0015	0.0015
Dielectric constant	4.25	3.1	1.85
Vacuum Dielectric constant	8.86E-12	8.86E-12	8.86E-12
Final Voltage (V)	1.33E+03	4.64E+03	1.24E+04

Table 5 shows the material properties and voltages that are generated between Teflon, a negatively charged material, and various positive triboelectric materials. The charge densities and the dielectric constants were averaged to perform these calculations. The calculations show that the lower dielectric constants are expected to have a higher voltage output. Teflon and Foam had the lowest dielectric constant of 1.85, and highest voltage output of 1240 V. Teflon with Cellulose had the highest dielectric constant of 4.25, and lowest voltage output of 133 V.

Procedure:

Eight materials were evaluated for their triboelectric properties. The positively charged materials chosen were Cellulose, Copper, Nylon, and Polyurethane foam, while the chosen negatively charged materials were Polyvinyl Chloride (PVC), Polytetrafluoroethylene (Teflon), Viton Fluoroelastomer Rubber, and Silicon Rubber. These materials were sourced from McMaster-Carr and are compiled in Table 6.

Table 6
Materials and Triboelectric Charge Density

Material	Triboelectric charge Density ($\mu C\ m^{-2}$)	Source
Positive		
Cellulose	46.5	(Li et al., 2023)
Nylon	283	(Liu et al., 2018)
Polyurethane foam	385	(Liu et al., 2018)
Negative		
Silicon Rubber	-69.95	(Zou et al., 2019)
Teflon (PTFE)	-113.06	(Zou et al., 2019)
PVC	-117.53	(Zou et al., 2019)
Viton Fluoroelastomer rubber	-148.20	(Zou et al., 2019)

Based on the charge densities displayed in Table 6, it is expected that the combination of Viton Fluoroelastomer rubber and Polyurethane foam would generate the highest voltage created due to repeated contact and separation of the two materials. The purpose of this experiment is to verify previous research on triboelectric materials while considering design specifications and future subject conditions.

6 x 6 inch samples of each material were prepared with a 6 x 6 inch strip of copper tape attached to the back of all eight samples. Each sample had an exposed wire placed between the triboelectric material and the copper tape. This allows the generated charge during testing to be conducted through the wire. The testing setup for the PVC film sample can be seen in Figure 12 below. For each trial, one positive and one negative material were paired and repeatedly tapped together with the contact occurring on the triboelectric material sides. Both wires were connected to an oscilloscope to measure the created voltage peaks. To ensure consistency of the results, one person wearing insulated plastic gloves conducted all the tests in one sitting while attempting to use the same amount of force to produce the motion and minimize the generated charge from dissipating. This setup allowed for repeated measurements, quantifying the triboelectric charge difference between each material pair.

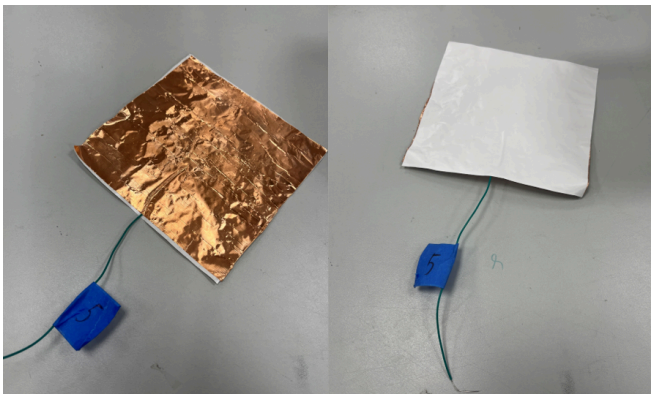

Figure 12: Primary Material Testing Setup for PVC Film Sample. Copper Tape Side (Left). Triboelectric Material Side (Right)

Results

The results after testing every available combination of positive and negative triboelectric materials are compiled in Table 7.

Table 7

Material Testing Results

	Cellulose	Copper	Nylon	Polyurethane foam
PVC	30-40 V; 55 max	9-12 V; 22 max	10-20 V; 35 max	20-25 V; 63 max
Teflon (PTFE)	35-45 V; 60 max	40-50; 85 max	40-50 V; 100 max	35-45 V; 50 max
Viton Fluoroelastomer rubber	15-20 V; 30 max	8-10; 20 max	50-60 V; 80 max	20-30 V; 40 max
Silicone rubber*	20-30 V; 40 max	-	10-20 V; 35 max	55-65 V; 102 max

*Note: Silicone rubber was sticky and took a longer, but still short, time to release from the opposite material

Of the 16 combinations shown in Table 7, three main categories can be created: 0-25 volts produced, 30-45 volts produced, and 50+ volts produced. The last category shows the most promise for maximum power generation. These combinations include: Nylon & Teflon, Nylon & Viton Fluoroelastomer Rubber, Teflon & Copper, and Polyurethane foam & Silicone Rubber. While copper was not found to create the most voltage, this material was selected as the positive material due to its simplicity for fabrication in the final design, through using copper tape.

There are possible errors associated with this testing arrangement. Human trials create variability in testing because it is difficult to manually apply a consistent force within a similar time frame for each trial throughout the experiment. This motion impacts the amount of voltage that is created and read by the oscilloscope. The created voltage is also impacted by potential differences in impact force and contact surface areas. Furthermore, the thicknesses of the

materials were slightly different, potentially leading to errors as the thicker materials may decrease the measured voltage.

For the blade material, we decided to use Thermoplastic Polyurethane (TPU) which is a flexible material that can be 3D printed for rapid prototyping and iterations. The specific TPU used was TPU-95A, a 3D printable plastic material. This TPU worked best for the 3D printers we have available. We could not conduct fatigue stress calculations, but the deflection calculations were promising. TPU-95A has a tensile modulus of about 26 MPa (UltiMaker, n.d.). Our team assumed the material would act the same in tension and compression. That led us to use the tensile modulus as if it were an elastic modulus. With that in mind, the elastic modulus of TPU-95A would be an order of magnitude lower than annealed 110 copper's. Assuming the material is isotropic and acts elastically for small deformations, a rectangular beam that was 15.24 cm tall, 2.54 cm wide, and 2.0 mm deep would deflect about 1.52 cm in 5 mph winds. This material's ability to deflect easily at low speeds led us to create multiple prototypes out of TPU and test it using the wind tunnel in the Mechanical and Aerospace Engineering building.

Final Specifications

Based on the results from the materials testing and other comparable technologies to our proposed solution, we developed the final specifications listed in Table 8.

Table 8

Functional Specifications (Final Specifications)

#	Specification	Metric(s)	Rationale
1	Voltage Generated per Surface Area of the Blade	Ideal: $4304 \frac{V}{m^2}$ Min: $1721 \frac{V}{m^2}$	When testing materials by hand, a 100 V max and a range of 40-50 V was found for Teflon and nylon film. The test area was 6 in. by 6 in. The ideal and maximum voltages per area was produced by dividing the maximum and lower bound voltages by the test area.
2	Sustained Power Generation	Ideal: 500 W Min: 100 W	The power generation of a generator with alternating current can be seen in equation (1) Our specification assumes the current is on the lower side of a typical solar panel at 10 A (ShopSolar, 2023). Using the equation given with our maximum voltage of 100 produced the ideal. The minimum was produced with our lower bound peak voltage, 40 V, divided by 2. The voltage was divided by 2 as 5 mph wind may not apply as much force as a person clapping.
3	Life Span	Ideal: 500×10^6 cycles Min: 300×10^6 cycles	In order for this product to be a worthwhile investment, it needs to last a long time. The ideal is based on the common number of cycles non-ferrous metals have their fatigue strength reported (Budynas, n.d.). The minimum is based on the fatigue strength found for annealed 110 copper.
4	Installation Cost	Ideal: $3.25 per Watt Max: $10.28 per Watt	Solar panel costs are typically measured as a cost per wattage. Solar panels in 2004 cost $10.28 per Watt (SaveOnEnergy, n.d.). Solar panels now in 2024 cost $3.25 per Watt (SaveOnEnergy, n.d.). Considering this is meant to fill a similar market, the pricing should be similar.

Table 9
Design Specifications (Final Specifications)

#	Specification	Metric(s)	Rationale
5	Current Form	Can produces direct current (DC)	While the power grid is based on alternating current, having the ability to convert the device's current to DC will allow for direct power to personal electronics
6	Optimal Wind Speed	Ideal: 5 mph Max: 8 mph	Wind speeds in Charlottesville are on average 5 to 8 mph (myPerfectWeather, n.d.).
7	Modular	Each power generation unit needs to be able to connect each other	Roofs vary in size and angle from home to home. To be as inclusive as possible, the design needs to be able to fit any roof size.

Table 10
Environmental Specifications (Final Specifications)

#	Specification	Metric(s)	Rationale
8	Environmental Resistance	Needs to be waterproof	If this product is going to be installed on roofs, it needs to be able to survive common weather events like precipitation.
9	Environmentally conscious	Needs be either compostable and/or recyclable	The purpose of this product is to produce a sustainable form of energy generation. If the product produces copious amounts of waste, it will negatively impact the environment and thus not be sustainable.
10	Safety	Ideal: Safety Factor = 2 Min: Safety Factor = 1.5	Because our device's loading is simple, there are well established mathematical models for our device. This allows for a lower factor of safety.

Electrical Setup

Repeated contact and separation of the two tribal materials creates voltages peaks, similar to alternating current (AC). This AC voltage is converted to a smoother, almost direct current (DC) like voltage output through the electrical system. This system uses a full wave bridge

rectifier to convert alternating current (AC) generated through the mechanical movement of the triboelectric system into direct current (DC). This voltage peak signal is sent through the copper wires which is, placed between the triboelectric material and the printed blade. This conductive copper backing collects and transmits the generated charge to the wires and into the electrical system.

The rectifier is in a closed-loop bridge configuration made of four diodes (Storr, 2013). This allows the current to flow in one direction for both the positive and negative, with the flow pattern being shown in Figure 13 below. This circuit allows for unidirectional flow of current for both half cycles. During the positive half cycle shown on the left of Figure 13, diodes 1 (D1) and 2 (D2) are forward-biased and conduct current while diodes 3 (D3) and 4 (D4) are reverse-biased (Storr, 2013). In this scenario where D3 and D4 are reverse-biased diodes, they act like a check valve, impeding the flow of current (*Forward Bias vs. Reverse Bias and Their Effects on Diode Functionality*, 2024). The functionality of these diodes is flipped in a negative half cycle (shown on the right of Figure 13), where D1 and D2 are now reverse-biased while D3 and D4 are forward biased, conducting current. The bridge takes the input waveform as seen at the top of Figure 14 and after rectification, results in a waveform where the voltage is all positive.

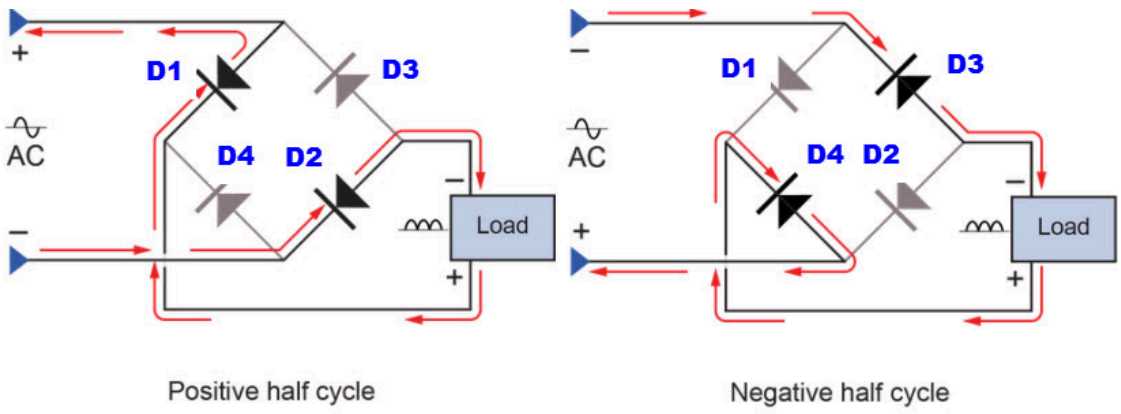

Figure 13: Positive and Negative flow through Rectifier bridge (Agarwal, 2014)

A capacitor connected in parallel with the rectifier has the ability to smooths the pulsating voltage peaks (*Half Wave and Full Wave Rectifier: Function, Comparison, and Applications | Electronics Basics | ROHM*, n.d.). The capacitor charges to the peak voltage during a ridge and discharges during the troughs. This reduces the fluctuation between the ridges and the peaks, creating a steadier DC output (Storr, 2013). For the final electrical set up, two 1.0 μF capacitors were placed in parallel. Capacitors in parallel add, this is effectively 2.0 μF. This increased capacitance allows for greater charge storage allowing for a smoother output voltage and minimizing the ripple.

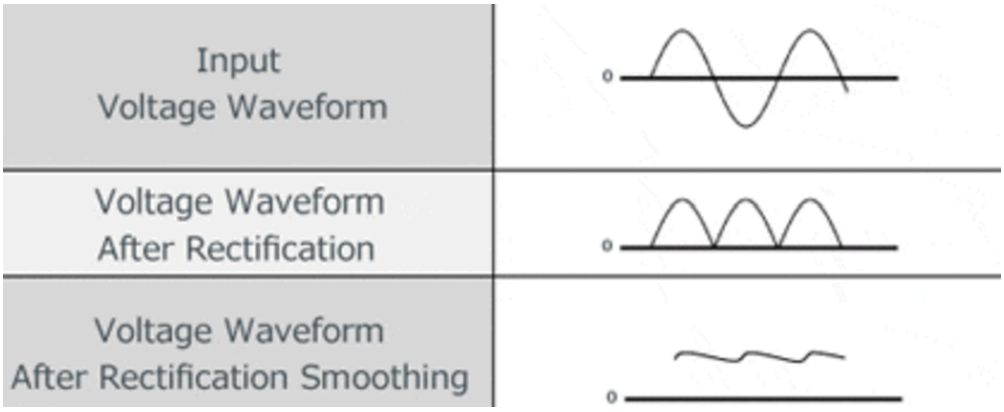

Figure 14: AC to DC Ripple Diagram (*Half Wave and Full Wave Rectifier: Function, Comparison, and Applications | Electronics Basics | ROHM*, n.d.)

The entire setup of the electrical components consisting of the bridge rectifier and capacitor will be assembled on a breadboard allowing for accessible prototyping. This will provide a solder-free solution for this part of the system. Through-hole components will be used,

to be placed on top of the breadboard. The modular design of the breadboard ensures that the electronic components can be easily removed for maintenance, ensuring longevity. A circuit diagram of the entire system can be seen in Appendix B, Figure 1.

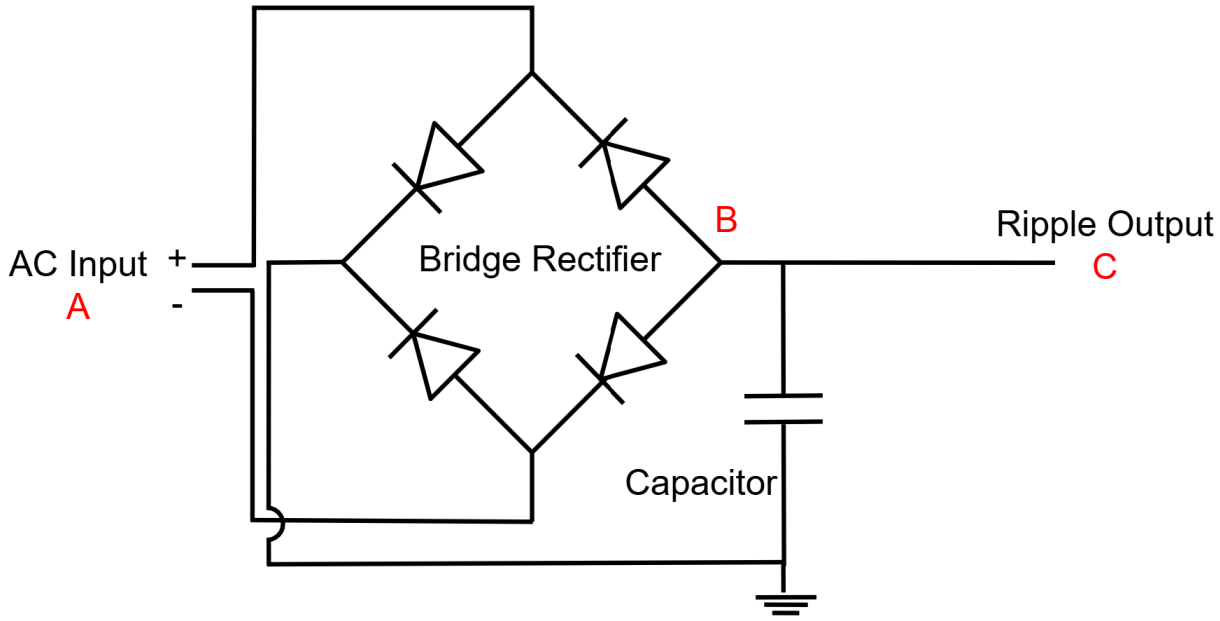

Figure 15: Converting AC to DC Electrical Circuit

At point A, displayed in Figure 15, the voltage waveform resembles the shape of the input voltage waveform that is collected from the positive and negative blades. This waveform undergoes the rectification process at point B and becomes a pulsating positive voltage waveform. Point C is after the smoothing process so the waveform transforms into a voltage that ripples horizontally, representing a DC signal with some fluctuations.This electrical system converts AC, generated by the triboelectric system, into stable DC using a full wave bridge rectifier and capacitor, creating a voltage output from mechanical movement. Two 1 μF capacitors were placed in parallel to give the smoothest ripple output during testing.

Design Prototyping

Phase 1: Early Testing with a Cylindrical Blade Design

Figure 16: Prototype cylindrical blades in and around the testing rig

Assumptions

Initially, our team developed a beam with a constant, cylindrical cross-section to act as the base of our triboelectric blades. These blades would be erected vertically on a building's roof to catch the wind and generate electricity. A cylindrical cross-section was chosen to limit the disruption of wind flow around them. Our assumption was a more bluff body would slow the wind down too much and prevent blades in the back of the array from bending.

These blades would have been encased by copper wires and a thin triboelectric material. For this analysis, the wrapping was assumed to be negligible as the thickness of the blade would be much greater. This will allow us to neglect the effect of the triboelectric material and copper wires on the strength of the beam overall.

Constant fluid density is assumed as the air is moving at subsonic speeds and is incompressible. Charlottesville also does not have significant variation in elevation. This means

the density of the air will not change significantly from place to place. Because of this, we assumed the density of air would be equal to its density at sea level. We also assumed the wind speed would be constant over the blade.

Calculations and Predictions

Using this model, the cylindrical blade's maximum distancing was found for Charlottesville's average wind speeds. The maximum distance between blades is determined by the maximum deflection found at the tip of the blade. The stress is important to ensure that the blades last long enough to be counted as a worthy investment for consumers wishing to install them.

To begin with, the distributed load from the wind was found using the drag force equation. Since the force is a distributed across the height of the beam, the drag force of the wind, F_D, was divided by the beam's height, h. This produced the distributed load, w, as seen in equation (3).

$$w = \frac{F_D}{h} = \frac{1}{2}\rho v^2 C_D A/h = \frac{1}{2}\rho v^2 C_D(a) \text{ (N/m)} \quad (3)$$

The force from the wind was found using the drag force equation. In this equation, ρ is the density of air, v is the velocity of the wind, C_D is the drag constant of the beam, and A is the projected cross-sectional area of the beam perpendicular to the wind. After replacing the cross-sectional area with its components, the height (h) and outer diameter (a) of the blade, the equation (3) for the distributed wind force was simplified. The density of air at sea level is $1.225\ \frac{kg}{m^3}$ (The Engineering Toolbox, n.d.). The drag force coefficient for a cylinder is 1.08 (Cao et al., 2014). These values were utilized to find the distributed loading for the beam type.

The reaction forces at the base of the blade were found by analyzing the beam as a static, cantilever beam with a distributed load, w, due to the wind. The free body diagram of the cylindrical blade subjected to this loading can be found in Appendix D as an example. Since the beam is static, the sum of forces and moments equal zero. The only applied force is in the negative x direction and is from the distributed wind force. This means the reaction force, R, is equal in magnitude to the total wind force as shown in equation (4).

$$R = hw = \frac{h}{2}\rho v^2 C_D(a) \text{ (N)} \tag{4}$$

The reaction moment, M, was found by summing the moment around the z-axis at the base. Since the reaction force is applied at the base, it runs through the point of rotation and can be negated. This means the reaction moment is equal in magnitude to the integration of the distributed wind force over the beam's height. This produces equation (5). In depth derivations can be found in Appendix D.

$$M = \frac{1}{2}wh^2 = \frac{h^2}{4}\rho v^2 C_D(a) \text{ (N-m)} \tag{5}$$

The deflection of the cylindrical blade was found using singularity equations. The equation (6) starts at the tip of the blade so that the reaction forces at the base do not need to be included. The distributed load from the wind is the only applied force on the blade. This produces equation (6) as the loading equation.

$$q(x_1) = -\, w\langle x_1 \rangle^0 \text{ (N)} \tag{6}$$

The variables for the set of axes used are x_1 and y_1 to show they are different from the original axes used to find the reaction forces. Upon integrating the loading equation, the

deflection angle and deflection equations were found to be equation (7) and equation (8), respectively.

$$EI\theta(x_1) = -\frac{1}{6}w\langle x_1\rangle^3 + C_1 \text{ (N-m)} \quad (7)$$

$$EIy_1(x_1) = -\frac{1}{24}w\langle x_1\rangle^4 + C_1x_1 + C_2 \text{ (Newton-meter squared)} \quad (8)$$

Where E is the Young's Modulus of the blade's material and I is the second area moment of inertia about the z_1 axis. The second area moment of inertia can be found based on the geometry of the cross-section. Equation (9) shows the second area moment of inertia for a blade with a hollow circular cross-section.

$$I = \frac{\pi(a^4-b^4)}{64} \text{ (m}^4\text{)} \quad (9)$$

In equation (9), a and b are the outer and inner diameters of the cross-section, respectively. The constants for equations (7) and (8) can be found by using the end conditions of the beam where $EI\theta(h) = 0$ and $EIy_1(h) = 0$. This is because the beam's base is fixed and the coordinate system currently being used starts from the tip of the beam. For the deflection equation, y_1 is isolated by dividing both sides by EI. After adding in the values of the constants and isolating $y_1$equation (10) is produced. In depth derivations can be found in Appendix D.

$$y_1(x_1) = \frac{w}{2EI}\left(-\frac{x_1^4}{12} + \frac{h^3x_1}{3} - \frac{h^4}{4}\right) \quad \text{(m)} \quad (10)$$

The fatigue life of this design was unable to be predicted analytically. Past research establishing the S-N (stress life) curve of this material could not be found. The only way we

would be able to determine the fatigue life of our design is through testing for hundreds of thousands of cycles. Due to time constraints, these tests were unable to be conducted.

The main considerations when creating this design were how far it would bend and if it would sway back and forth in the wind. The three factors that would be altered when making the blade would be its height, outer diameter, and inner diameter. The heights of the cylindrical blades were made to be 15.24 centimeters (6 inches) or less because the triboelectric material that would encase them were cut by the manufacturer into 6 inch by 6 inch squares. Using equation (10), the deformation of the cylindrical blade was predicted to be less than a centimeter unless the outer diameter was about 3.4 millimeters or less. This outer diameter would have been too small to be useful for triobelectricity generation, so a larger diameter was used for all cylindrical designs tested. While this meant the blade would have little deformation, the design was tested to find if it could oscillate in the wind.

There were 2 considerations when designing the blade: The fatigue stress it experiences from bending in the wind and the deflection of the blade's tip. The fatigue stress on the blade depends on the extreme wind speeds it may encounter. Our team wanted our design to be able to withstand 60 mph wind speeds, a "very low" description from NOAA's severe wind threat level descriptions (NOAA, n.d.). The deflection of the blade is used to determine the maximum distance we can place them in the prototype. This is dependent on the lower bound for Charlottesville's average wind speed of 5 mph (myPerfectWeather, n.d.).

From these calculations it was found that copper would not be able to meet both metrics on its own. In order for annealed 110 copper to bend in low wind speeds, it would have to be very thin. This is due to its large elastic modulus at $118\ kN/mm^2$ or 118 MPa (Chapman, 2016). But to avoid breaking in the event of high winds, the beam would need to be so thick it would be

effectively rigid in all wind speeds. One configuration that was considered was a beam 0.1524 m tall, 0.0254 m wide, and 0.000127 m deep with a rectangular cross-section. For such a design, the beam would deflect about 1.311 cm in 5 mph winds. In 60 mph winds, though, the beam would experience about 2.437 GPa of stress which exceeds the established maximum stress. If copper is to be used, a mechanism would need to be used so that the leaves could be sheltered from extreme wind speeds.

Testing

To test the cylindrical designs, they were put in a wind tunnel and subjected to wind speeds varying from 5 mph to 20 mph. Blade deformation was measured using a ruler fixed along the side of the wind tunnel's glass wall. The oscillation range of the blades under wind flow was estimated by analyzing video recordings, using the ruler as a reference scale for displacement.

Results

The cylindrical blades were found to be too stiff to deflect and showed little oscillations in the wind. Even the thinnest of blades held straight when subjected to the 5 mph wind speeds typical to Charlottesville. When subjected to 30 mph winds, the blade would only deform 3 to 5 cm. On top of this lackluster deformation, the blades did not oscillate in the wind. No matter how fast or slow the wind speed was, the cylindrical blades would vibrate a negligible amount after deformation.

Our team predicted the lack of deformation and oscillation was due to the cross-section of this blade design. In order to make the blade more flexible, the outer diameter would have to be decreased and the inner diameter increased. Such a change would decrease the blade's second area moment of inertia. As can be seen in equation (10), a decrease in the second moment area of

inertia should create an increase in deflection. The inner diameter cannot be increased too much as the TPU-95A filament's thickness creates a minimum thickness for the cylinder. This means decreasing the outer diameter would be the main method to change the second moment area of inertia The problem with this cross-section is that a decrease in the outer diameter would also decrease the load applied by the wind. This can be seen in equation (2). These changes in blade stiffness and applied loading would then cancel each other out and create little change in blade's deformation in the wind. In order to avoid this, we went on to consider designs which could have the second area moment of inertia decreased without changing the load applied by the wind.

Phase 2: Refining Prototype Using a Flat Blade Design

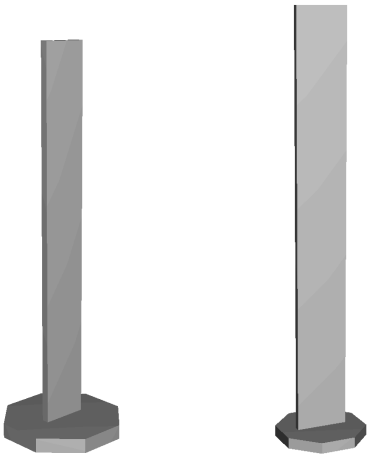

Figure 17: Computer aided design models of the flat blade used

Assumptions

The flat blade design was considered because its second area moment of inertia could be decreased by changing the thickness of the blade. This change would not affect the load applied to the beam as its width, which generates the drag force, would remain unchanged. Our team assumed this design would disrupt wind flow more than the cylindrical design due to it being

more bluff. But, we assumed these designs would allow for more spacing between blades so that the wind speed would be about constant throughout their array

The assumptions previously made for the cylindrical blade's orientation, wrapping, and fluid density have also been made for this design.

Calculations and Predictions

The equations previously used for the cylindrical blade were also applied to this design. The only difference between the two being their dimensions and second area moment of inertia. The variable "a" in the equations for the distributed load on the beam, the reaction force, and the reaction moment was changed to be the width of the beam. The second area moment of inertia for a beam with a full, rectangular cross-section was found to be equation (11). In this equation, a is the width of the blade which is perpendicular to the wind and b is the thickness which is parallel to the wind. Using equation (11) and (10), it was found that the width of the flat blade would not impact the deflection of the blade.

$$I = \frac{ab^3}{12} \text{ (m}^4\text{)} \tag{11}$$

On top of finding the displacement of the blade's tip, natural frequencies of the blade were predicted analytically. In order to maximize the oscillation of the blade, our team wanted the natural frequency of the blade to be close to its vortex shedding frequency. The vortex shedding frequency of the blade can only be found through testing. In order to maximize the chance of creating a blade with a natural frequency close to its vortex shedding frequency, our team created a slew of blades with a wide range of natural frequencies. Because this design, the natural frequency of the blade's tip (first mode natural frequency) and the of the blade's center (second mode natural frequency) were predicted using equation (12)

$$\frac{K_i}{2\pi}\sqrt{\frac{EIg}{wh^4}}\ (\text{hz}) \qquad (12)$$

In this equation, K_i is the constant used for the natural frequency being calculated with the i being the number of the mode. The K-constant for first and second mode natural frequency for this beam is 3.52 and 22, respectively. E is for the Young's Modulus of the material is E, I is the second area moment of inertia of the cross-section, g is gravitational acceleration, w is the distributed load from the wind, and h is the height of the beam. Using this equation, it was once again found that the width of the flat blade did not impact the natural frequency it experienced.

Testing

The flat blades were tested in a wind tunnel and subjected to varying speeds like the cylindrical blades. Unlike the cylindrical blades, the speed was varied to determine the blades' natural and vortex shedding frequencies. The blades' deformation and oscillation in the wind tunnel were recorded using a high speed camera so it could be analyzed later using Pixelink Capture Software. The deflection of the blades' tips at the different wind speeds was also documented using a ruler attached to the side of the wind tunnel glass. There were 3 batches of flat blades tested. The first batch had 4 blades with a constant height of 15.24 cm and variance of thicknesses. The widths remained the same across the blades. The second batch had 12 blades which varied in thickness and height, but not width. The width remained the same as in the first batch. The third batch also varied in thickness and height, but not width. The width in this batch was increased. For the tables illustrating the dimensions of these flat blades, see to Appendix E. The first batch was tested to determine the blades' deflection in the wind. The second and third batch were tested in an attempt to create designs with overlapping natural frequencies and vortex shedding frequencies.

Results

For the first batch of tested blades, A1 buckled from its own weight and did not move from the wind in the tunnel. Blade D1 did not move because it was too stiff for low wind speed. Blades B1 and C1 did not deform past 1 cm in the wind, but did oscillate with an amplitude of 1 mm. These tests were carried out before the frequency of the blades were taken into account. Because of this, the main point of improvement made between batch 1 and 2 was to decrease the height such that the blades would not buckle.

For the second batch, the deflection and oscillations seen by the blades were much smaller than the first batch. Blades A2, A3, and A4 all deflected and oscillated at the tip more than the other designs, but still had an amplitude within 1 cm. It was believed that this was due to the designs having the lowest mode 1 natural frequencies of the second batch. There was no movement at the centroid of the blades, which led to the assumption that the mode 2 natural frequency was too high to be a factor in the designs oscillating. From this information, the third batch of blades were made to have a drastically lower natural frequency. For reference, blade A4 had the lowest first mode natural frequency of the second batch at about 2.935 Hz. In the third batch, the lowest first mode natural frequency was A7 at 1.252 Hz.

Only two thirds of this batch were printed and tested with blades A5, B5, C5, and D5 being excluded due to time constraints. From this batch, it was found that once again the blades with the lowest first mode natural frequencies were the ones to oscillate the most. Blade D6 and D7 oscillations had an amplitude of about 1 cm in the wind. Meanwhile, blades A6 and A7 oscillated with an amplitude of about 2 cm in the wind after deforming about 8 cm at the tip.

From these tests, our team was able to determine that the designs moving forward would have to be thin and tall in order to oscillate in the wind enough to produce the force needed for

triboelectric energy generation. On top of this, the design would need a more sizable area for the triboelectric materials to make contact with one another. This is because the oscillations would not be substantial at low wind speeds. To compensate for that, more material would need to be in contact with every oscillation of the beam. While the flat blade could be made thinner and taller to oscillate more in the wind, increasing the width for more triboelectric material to be too disruptive of the wind flowing around it. The goal was to have these designs in an array. If this blade was much wider, it would block the wind from moving to the blades further back in the array. Because of the limited surface area allowed on the flat blade design, it was retired for the final design which appeared to address these concerns.

Final Design Development: The Leaf Generator

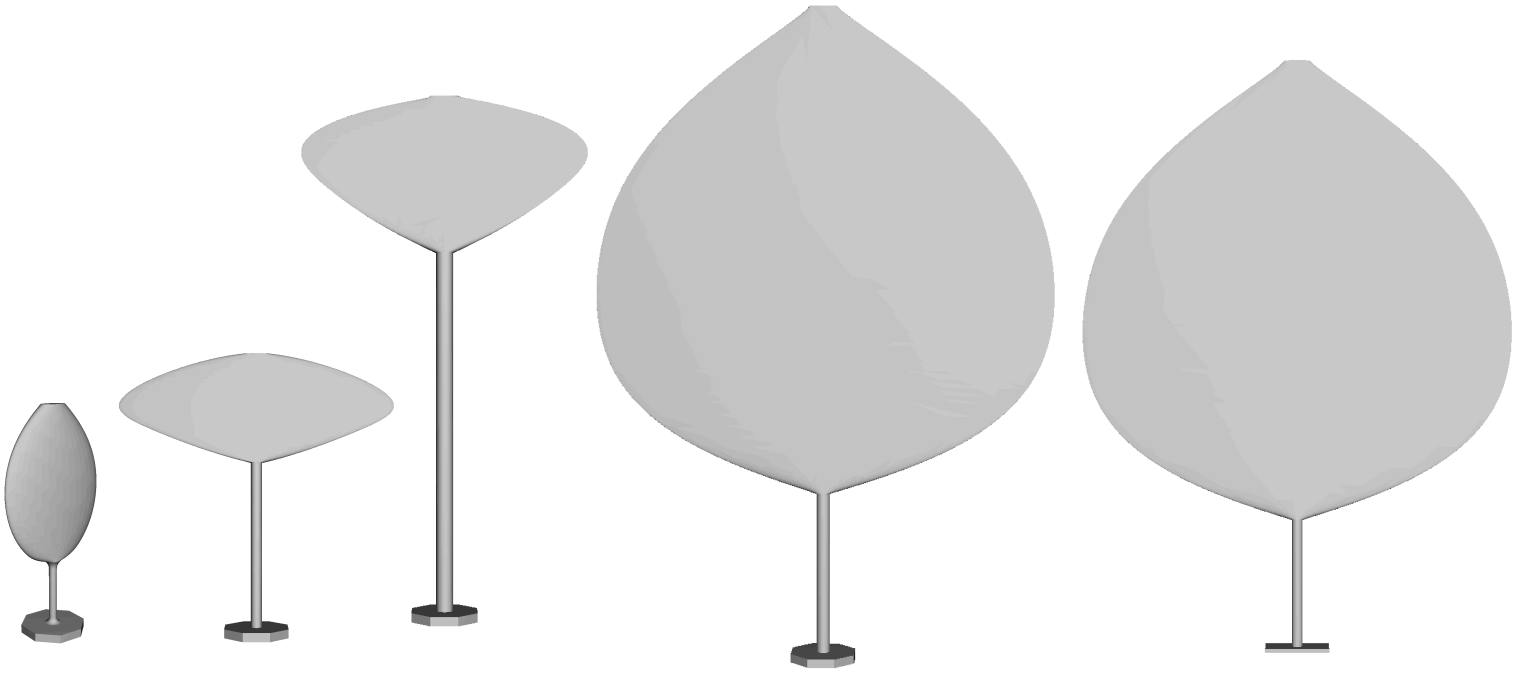

Figure 18: Development of Leaf Designs. (From left to right) Gen 1, Gen 4, Gen 4, Gen 6, Gen9.

Assumptions

After the tests with flat blade designs, the advantages of increased surface area for enhancing drag force became evident. This insight led to the development of the leaf-inspired concept shown in Figure 18. The design was divided into two components: a solid cylindrical stem at the base and a wide, ellipsoidal plate above. The stem was modeled as a vertical cantilever beam subjected to a distributed load along its length and a point load at the tip. To model the forces on the leaf, a drag coefficient of 1.08, corresponding to a cylinder, was applied to the stem. For the leaf section, an ellipsoidal plate drag coefficient of 1.17 was used. As with previous designs, fluid density was assumed constant due to subsonic, incompressible airflow. Air density was assumed to be at sea level, and wind speed was assumed to remain uniform across the device.

Calculations and Predictions

Geometric and stress calculations.

$$A_{Leaf} = \frac{1}{2} \pi r_{Leaf} h_{Leaf} \tag{13}$$

Equation (13) calculates the surface area of the leaf plate. We initially used the standard surface area formula for an ellipsoid ($A = \pi r h$). However, after comparing the theoretical values to the actual surface areas obtained from SolidWorks, we introduced a leading coefficient of ½ to better align the calculated values with the modeled geometry.

$$P = \frac{1}{2} \rho v^2 C_{D\,Leaf} A_{Leaf} \tag{14}$$

Where P is the point load on the tip of the stem due to leaf drag force. $C_{D\,Leaf}$ is assumed to be 1.17, v is the inflow velocity (m/s), and ρ is air density at sea level (1.225 $\frac{kg}{m^3}$).

$$w = \frac{1}{2}\rho v^2 C_{D\,Stem} h_{Stem} \quad (15)$$

Equation (15) defines w as the distributed load on the stem due to drag force. $C_{D\,Stem}$ is assumed to be 1.08, and h_{Stem} is the vertical height of the stem cylinder.

$$I = \frac{\pi d_{Stem}^4}{64} \quad (16)$$

Equation (16) defines I as the second area moment of inertia for a cylinder, where d_{Stem} is the diameter of the stem cylinder.

$$\theta = -\left(\frac{P}{2\,E\,I}\right) + \left(\frac{w}{6\,E\,I}\right) \quad (17)$$

Where theta is the angular deflection of the stem. The coordinate system is defined with its origin at the free end of the cantilevered stem to eliminate the need to account for reaction forces. E represents the Young's Modulus of the TPU-95A material (26 MPa).

$$\delta_{Stem} = \left[\left(\frac{P}{6\,E\,I}\right) + 2h_{Stem}^3\right] + \left[\left(\frac{w}{24\,E\,I}\right) + 3h_{Stem}^4\right] \quad (18)$$

Equation (18), derived from the Euler-Bernoulli beam equation, calculates the displacement on the tip of the stem from the distributed load and point load. Again, the coordinate system is defined at the free end of the stem to eliminate the reaction forces.

$$\delta_{Leaf\,Tip} = \delta_{Stem} + h_{Leaf}\,sin(\theta) \quad (19)$$

Equation (19) determines the maximum displacement, located at the tip of the leaf. The leaf section is assumed to be rigid and unbending. The total displacement is derived from the stem tip's displacement, its angular deflection, and the vertical height of the leaf.

$$\sigma_{xx} = \frac{[(P\, h_{Stem}) + 0.5(w\, h_{Stem}^2)] \cdot 0.5\, d_{Stem}}{I} \quad (20)$$

Equation (20) determines the bending stress on the stem, parallel to the wind direction.

$$B_{Leaf\ crit} = \frac{\pi^2 E\, I}{4h_{Stem}^2} \quad (21)$$

Equation (21) determines the critical buckling load on the stem.

$$B_{Leaf} = 9.81 \cdot \rho_{TPU} A_{Leaf}\, t_{Leaf} \quad (22)$$

Equation (22) determines the applied buckling load on the stem, which is equivalent to the weight of the leaf, where ρ_{TPU} is the density of the TPU material (1220 $\frac{kg}{m^3}$), and t_{Leaf} is the thickness of the leaf section.

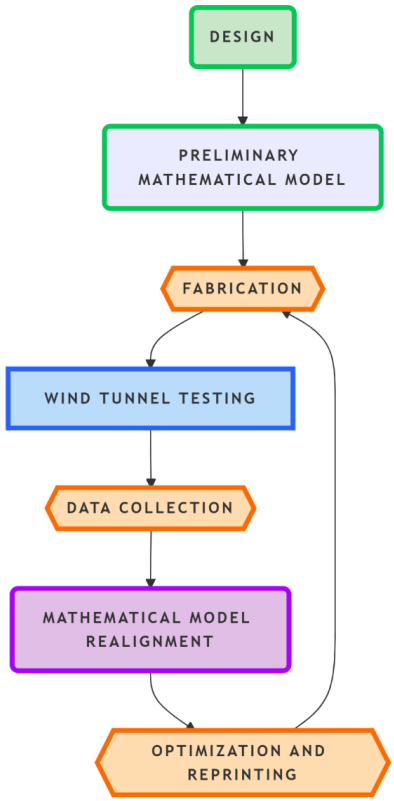

Figure 19: Iterative Leaf Design Process

The initial designs of the 3D-printed triboelectric harvesting leaves (Generations 1–3) were developed based on fundamental theory, background research, experimental observations, and preliminary deflection and fatigue calculations. These early iterations focused on validating basic design principles and understanding material behavior under cyclic loading. Beginning with Generation 4, we shifted to a more systematic and data-driven approach by implementing a MATLAB optimization script, available in Appendix F and Appendix G. This tool generated ideal candidate designs based on weighted performance criteria and geometric constraints. In addition to the weighted performance criteria, the script filtered out any models meeting or exceeding certain criteria relating to fatigue, including bending, displacement, and buckling.

When verifying the results of the MATLAB code, as seen in Appendices G and H, Finite Element Analysis (FEA) in SOLIDWORKS was an important tool, producing similar results in terms of deflection and stress, as shown in Figure 20. When testing, the blades behaved similarly to these simulations, verifying the models used.

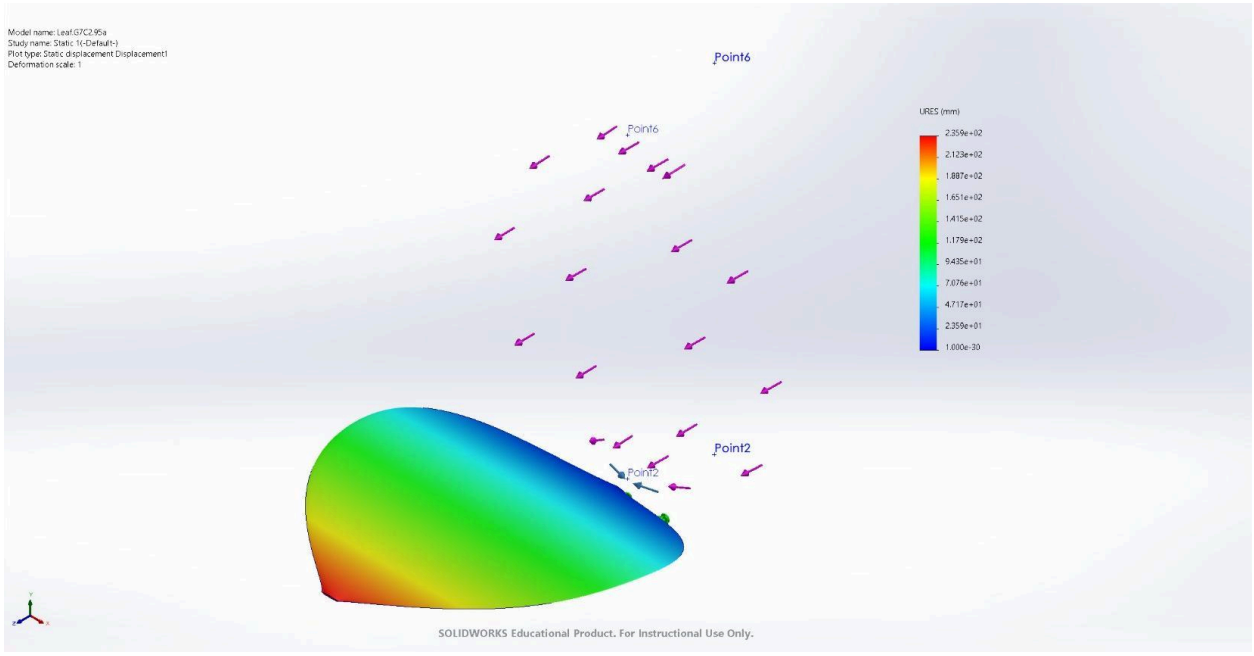

Figure 20: FEA of Leaf Deflection

Each design was modeled in SolidWorks, fabricated using 3D printing, and tested in a wind tunnel. Test results informed updates to our theoretical models and design assumptions, which were then used to refine the optimization algorithm. This iterative process, shown in Figure 19, led to steady improvements in prototype performance throughout Generations 5–9, ultimately resulting in the final design seen in Figure 21.

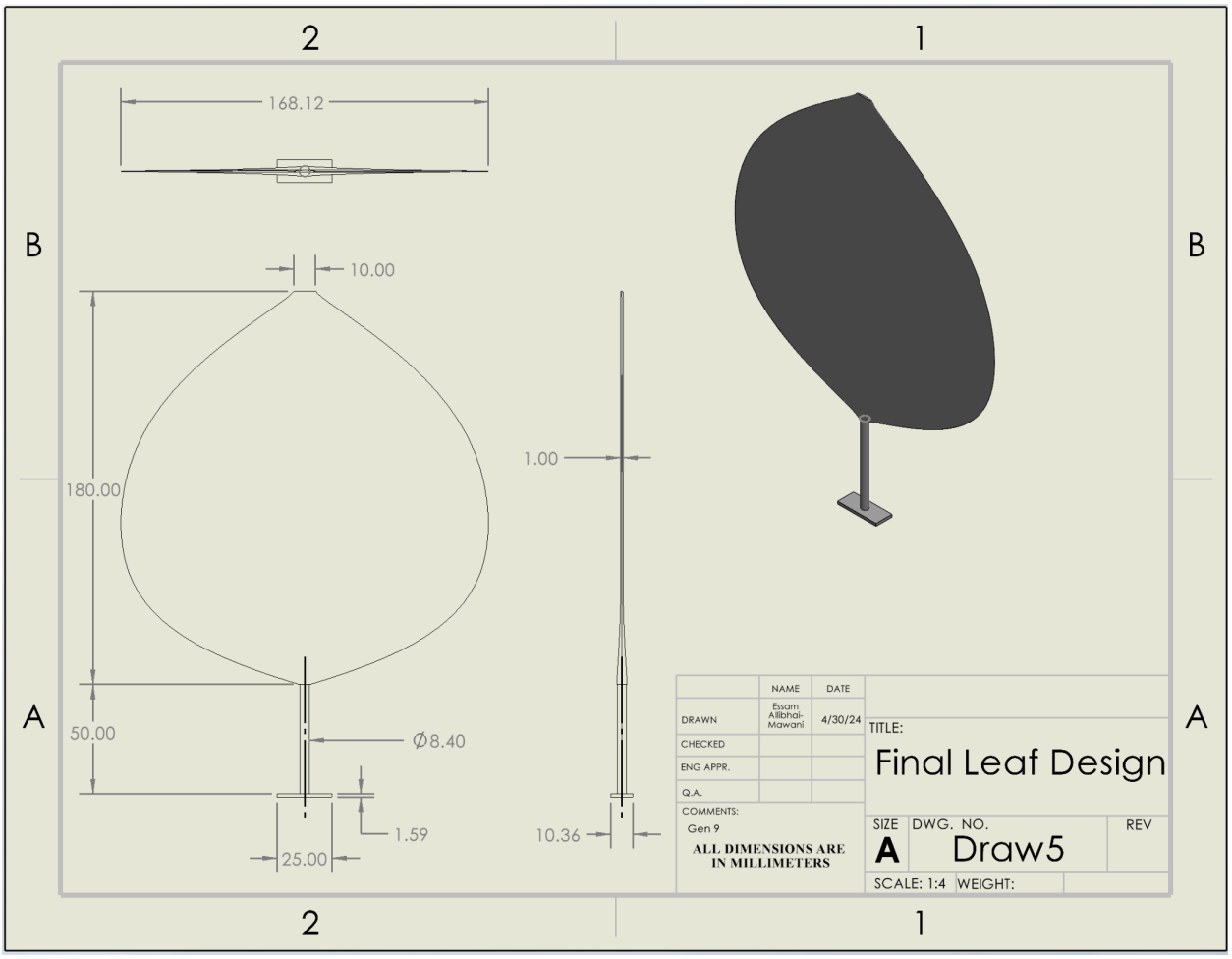

Figure 21: Dimensions of Final Leaf Design

Refining Performance through Frequency Analysis.

In further iterations of the design, a large emphasis was placed on inducing vibration through matching frequencies. Due to the complex geometries, the natural frequency of the leaves needed to be calculated through Finite Element Analysis. The FEA was performed in SOLIDWORKS and output the 6 modal frequencies associated with the 6 degrees of freedom of the object. Table 11 shows the frequencies for the final design, including a natural frequency of 1.18 hertz.

Table 11:

Frequencies of the Final Design

Modal Frequency	Rad/sec	Hertz	Seconds
1	7.4527	1.1861	0.84307
2	11.416	1.8169	0.55038
3	17.089	2.7199	0.36767
4	28.39	4.5184	0.22132
5	48.552	7.7272	0.12941
6	66.003	10.505	0.095195

In order to induce vibrations, a forcing frequency would have to interact with the object consistently with a value equal to its natural frequency. Although there are 6 modal frequencies, the 1st mode frequency results in the most amplitude. When an object is in laminar flow, a wake typically forms with consistent geometries and shedding. This wake consists of vortices which shed off the object at a constant rate, which is called the vortex shedding frequency. The current leaf design (Figure 21) has a characteristic length of 16 centimeters, requiring a high wind speed for the vortex shedding frequency to match the small natural frequency of the leaf and cause increased amplitude on the oscillations. The high wind speeds required are contrary to the aim of the project. The formula for strouhal number can be seen in equation (23). The strouhal number is typically 0.2 for a cylinder and 0.16 for a flat plate (Radi et al., 2013; Rostami et al., 2019).

$$St = \frac{fL}{U} \tag{23}$$

In equation (23) above, f is the frequency (hz), L is the characteristic length (m), U is the velocity (m/s), and St stands for the strouhal number. To decrease the wind speed required for large oscillations, the leaves were redesigned to be stiffer and lighter (Figure 22). Taking into consideration that the strouhal number of a flat plate is 0.16 and the characteristic length is 16 cm (0.16 m), the resulting frequency is roughly equal to the wind speed in meters per second (4 m/s

mentioned in Literature Review section), which equates to around 4 hz. The resulting prototypes had thicker stems and were designed to have a natural frequency of around 4 hz, shown in Figure 22. The faces of the leaves were left out of the design, as they lowered the natural frequency by a large margin. In order to achieve a large contact area, the thin (~0.05 mm) triboelectric materials were glued onto the stem to achieve a leaf-like shape. These leaf faces maintained the large geometries of the previously designed leaves, having a height of 15.25 cm and a height of 16 cm, ensuring a strouhal number of 0.16 and therefore a vortex shedding frequency of 4 hz. Theoretically the matching vortex shedding frequency and natural frequency should induce resonance in the leaves.

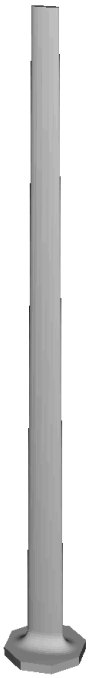

Figure 22: Vortex Shedding Stem Design

In order to confirm the vortex shedding frequency of a flat plate with a characteristic length of 16 cm, a computational fluid dynamics simulation was performed, with confirmation of the vortex shedding frequency of 4 hz, shown in Figure 23.

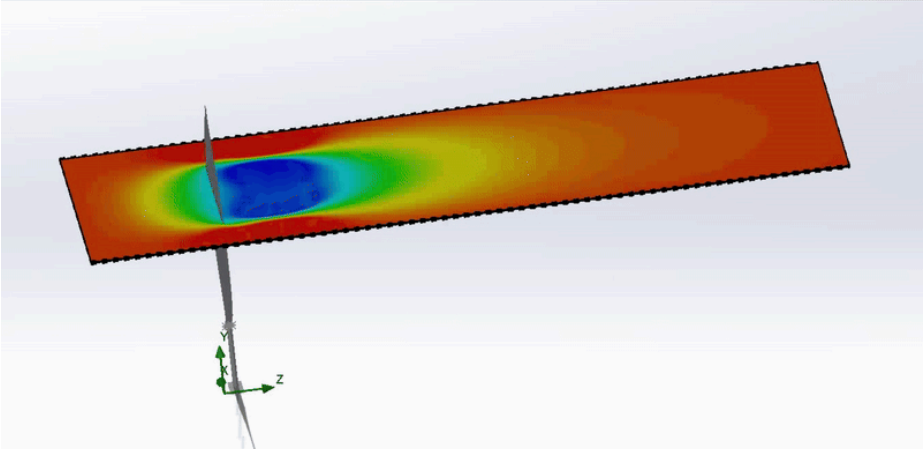

Figure 23: Fluid Dynamic simulation video

In addition to the visualization, the Computational Fluid Dynamics (CFD) program outputs data points throughout the simulation shown in Figure 24. The first 2 seconds show a frequency of 4 hz, as there are approximately 4 peaks per second. However after the first 2 seconds there is much smoother wake.

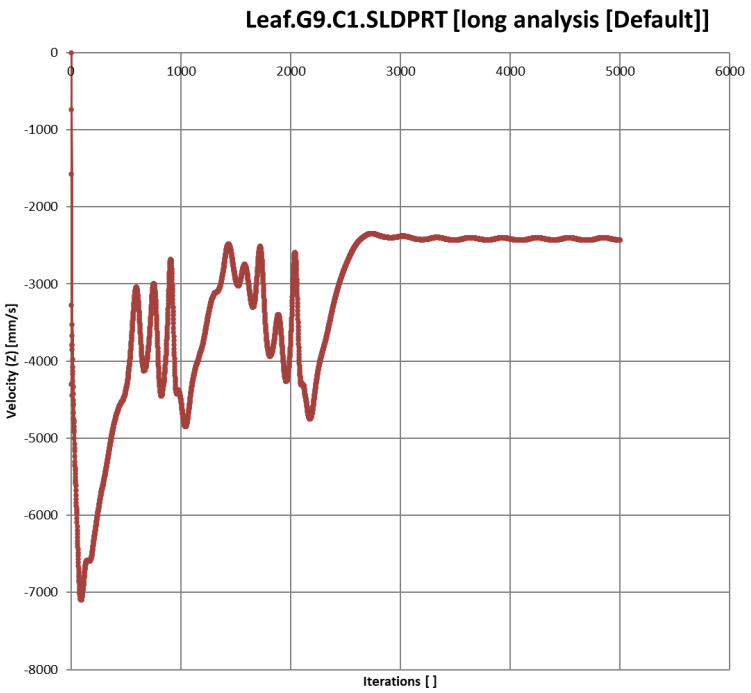

Figure 24: Graph showing CFD vibrations

Testing

To evaluate the performance of our triboelectric leaf prototypes, we carried out a series of tests in a controlled wind tunnel environment. These tests were used to verify the basic functionally of the designs, while also evaluating deflection behavior, vibrational stability, dynamic interactions, and electrical output under realistic operating conditions. The results provided valuable feedback that helped guide further improvements in refining our design. A 3D printed rigid PLA testing rig (Figure 25) enabled a rigid connection to the floor for the flexible TPU leaves. The base was designed to enable testing in 45 degree increments with octagon connections between the testing rig and the leaves. In addition to this, the testing rig was designed to hold an array of 3x3 leaves to test different groups of leaves, seen in Figure 25.

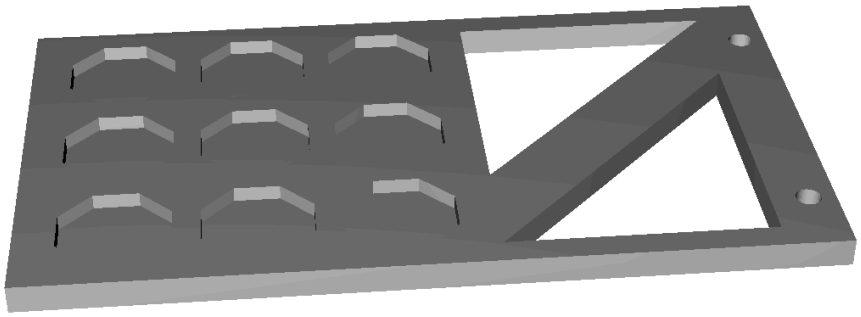

Figure 25: PLA Testing Rig

Prior to a full system testing, we conducted preliminary tests on the individual blades to test their deflection and frequency in different wind speeds. Each leaf design was tested separately in wind speeds ranging from 5-30 mph and recorded by a high USB3 Vision PL-D series high speed camera and Pixelink Capture Software that enabled us to record the deflection and frequency of each leaf. This data was then used to iterate through designs until there was a design that had a large amplitude when it oscillated.

The second test consisted of two blades placed at different distances between each other with a goal of analyzing the dynamics of multiple leaves. The leaves had triboelectric material taped to them, copper on one and teflon on the other. The electrical setup shown in Figure 15 was attached to the two leaves to convert the voltage generated by the leaves into DC current. One wire went into the positive terminal of the bridge rectifier and one went into the negative. Figure 26 shows the testing setup. Leaves were analyzed for the oscillations between the two of them, the amplitude, and the voltage created from the collisions.

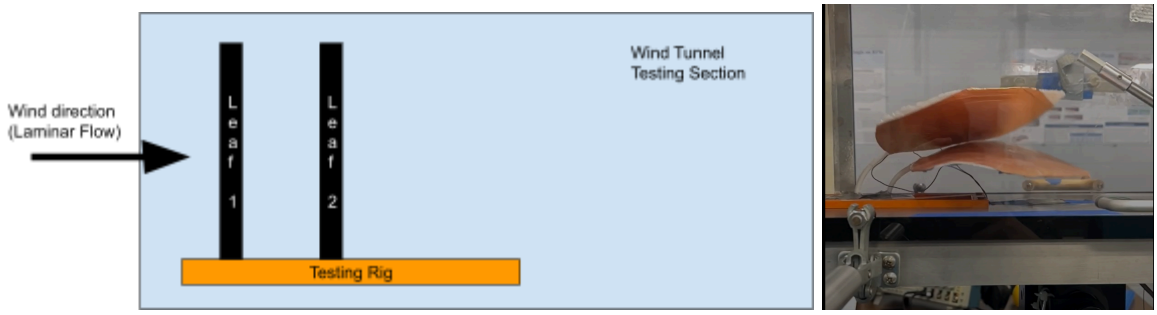

Figure 26: Diagram (left) and picture (right) of testing setup

The third test consisted of three leaves back to back to back in a similar manner to the two leaves and attaching the electrical setup to the three leaves. Testing consisted of varying the wind speeds and orientation of the leaves, observing the oscillations of the leaves and measuring the voltage created from the collisions. The voltage ended up not being significantly greater than the two leaf test.

We also tested if we could induce frequencies in the leaves via vortex shedding. Our initial test consisted of placing a uniform object placed upstream of the leaves to induce a vortex shedding frequency (Figure 27). The goal of this experiment was to test how the leaves reacted to an induced frequency.

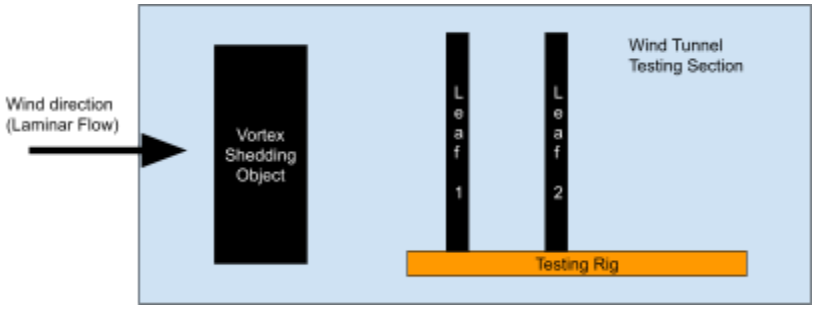

Figure 27: Vortex Shedding Wind Tunnel Set Up

During these tests, videos of the leaf vibrations were collected using a USB3 Vision PL-D series high speed camera and Pixelink Capture Software. Postprocessing of the videos in

MATLAB provided the position and frequency of the blades. When analyzing these vibrations, two sets of data were collected, one was with no object downstream and the other had an object downstream. Appendix H provides the code used to analyze the results.

Figure 28: Testing setup for Vortex Shedding of Leaves

Final tests consisted of an attempt to match the natural frequency with the vortex shedding frequency. Figure 28 shows the setup used for these tests. The upstream leaf was placed to induce vibrations in the downstream leaf. Throughout all tests, electrical components were connected, and an oscilloscope was used to monitor and record the voltage output generated by the system.

Results

Electrical

Within the wind tunnel during the two leaf testing, at a wind speed of 19 mph (a rotational speed of 500 RPM), voltage peaks generated from contact separation events between conductive elements were recorded, with peak amplitudes ranging from 35 to 60 V. After processing through the electrical setup, the system produced a nearly constant DC output of approximately 100 mV. Increasing the speed to 21 mph (550 RPM) resulted in peak voltages between 50 and 70 V, with a high DC output of 120 mV. At 23 mph (600 RPM), voltage peaks further increased, ranging from 60 to 95 V, where DC output only increased slightly to about 130 mV compared to the 550 RPM reading.

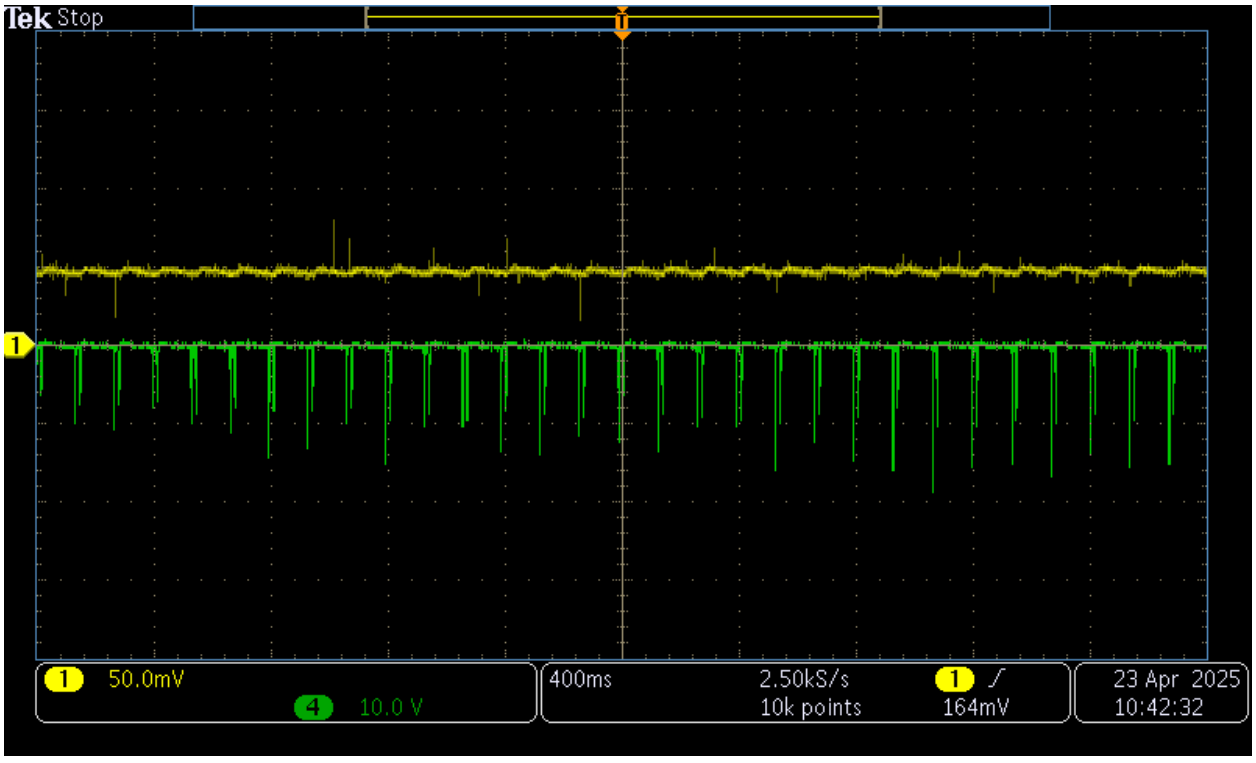

Figure 29: Voltage Peaks (Green) and Output Voltage (yellow) for two blades at 19 mph

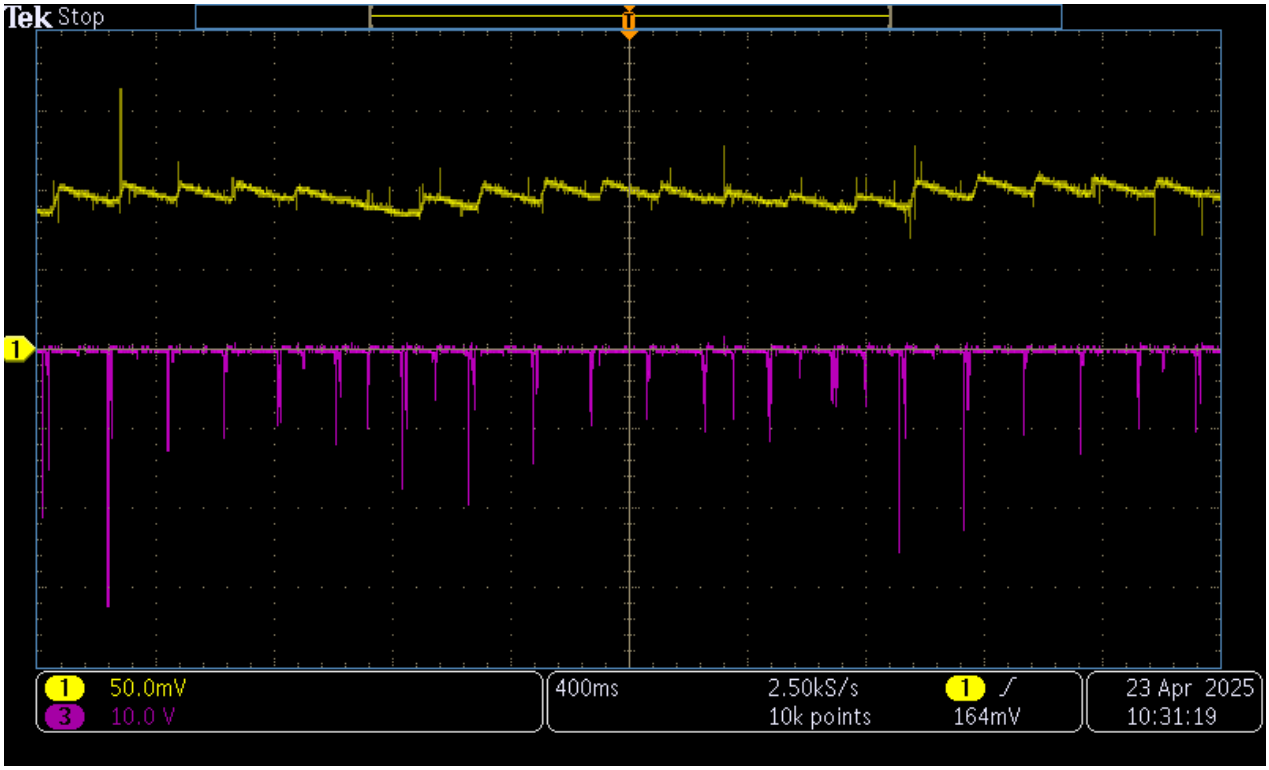

Figure 30: Voltage Peaks (Pink) and Output Voltage (yellow) for two blades at 21 mph

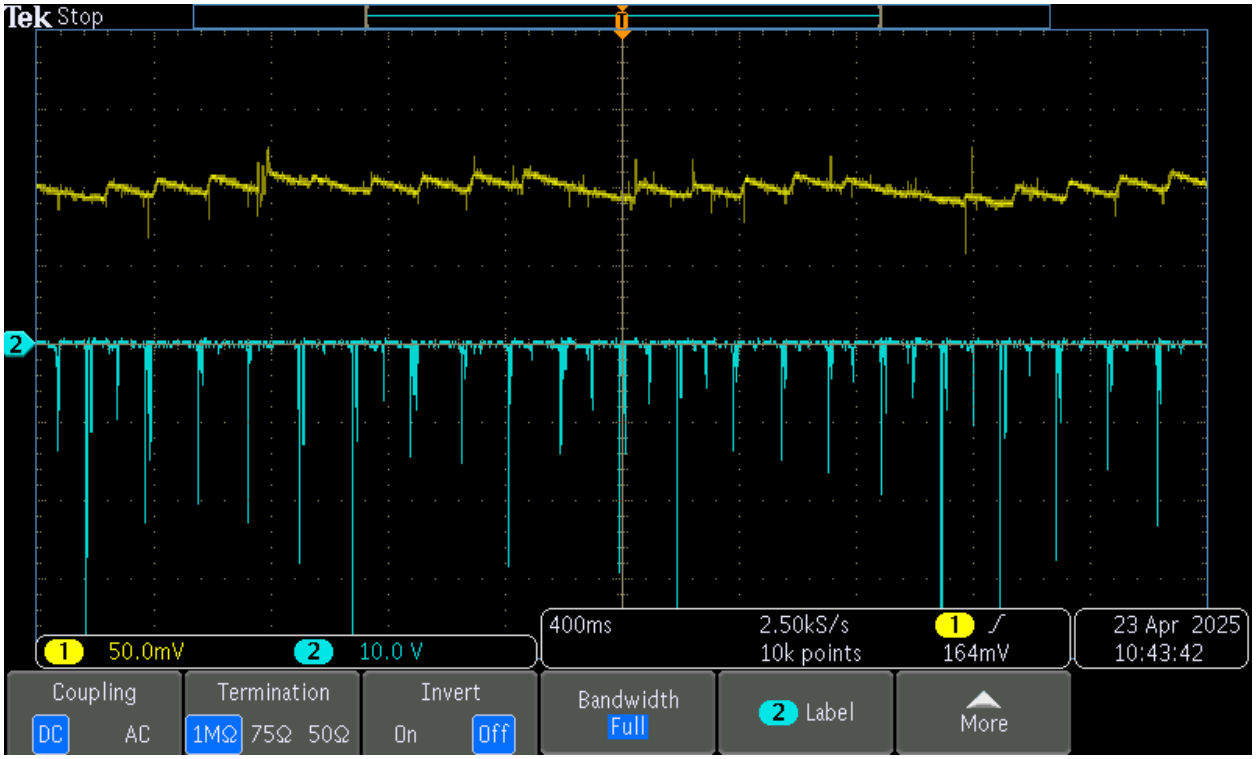

Figure 31: Voltage Peaks (blue) and output voltage (yellow) for two blade system at 23 mph

Dynamic

When experimental results were analyzed, minimal vibrational response was seen at lower wind speeds, but as speed increased, vibrational response increased. When 2 leaves were tested, there was much more vibrational interaction compared to when 3 leaves were tested in a row. This is most likely attributed to the weight of the face of the leaf and the flexible stem. When the vortex shedding frequency inducing object was placed upstream, there didn't seem to be a correlation. Appendix I shows the frequency output of the leaf when different frequencies were induced, visualizing the incongruence. Qualitatively, it seems that the leaf needed a constant forcing frequency on it to get consistent motion. This applied to both the stiff leaves and the flexible leaves, when they touched each other little vibration occurred, however when separated vibrations of the leaf occurred. This is shown in Figure 32. However the amplitude of vibrations were too small to reach the wide gap between leaves needed to induce a vortex shedding frequency.

Figure 32: Video of Vibrations

Exploring Alternatives: The Pinwheel Generator

Alongside development of triboelectric leaves, another design showed signs of success. Similar to a traditional wind turbine, the pinwheel generator harnesses energy by spinning a series of blades. In a typical turbine, these spinning blades would rotate a shaft used to power a generator. This design lowers operating wind speed and minimizes moving parts by using triboelectric material at the ends of the blades to contact an opposite triboelectric material attached to the base. A conductive wire connects the two materials, and a slip ring is used to prevent wire twisting as the blades spin. This experimental set up successfully achieved voltage spikes caused due to repeated contacts in wind.

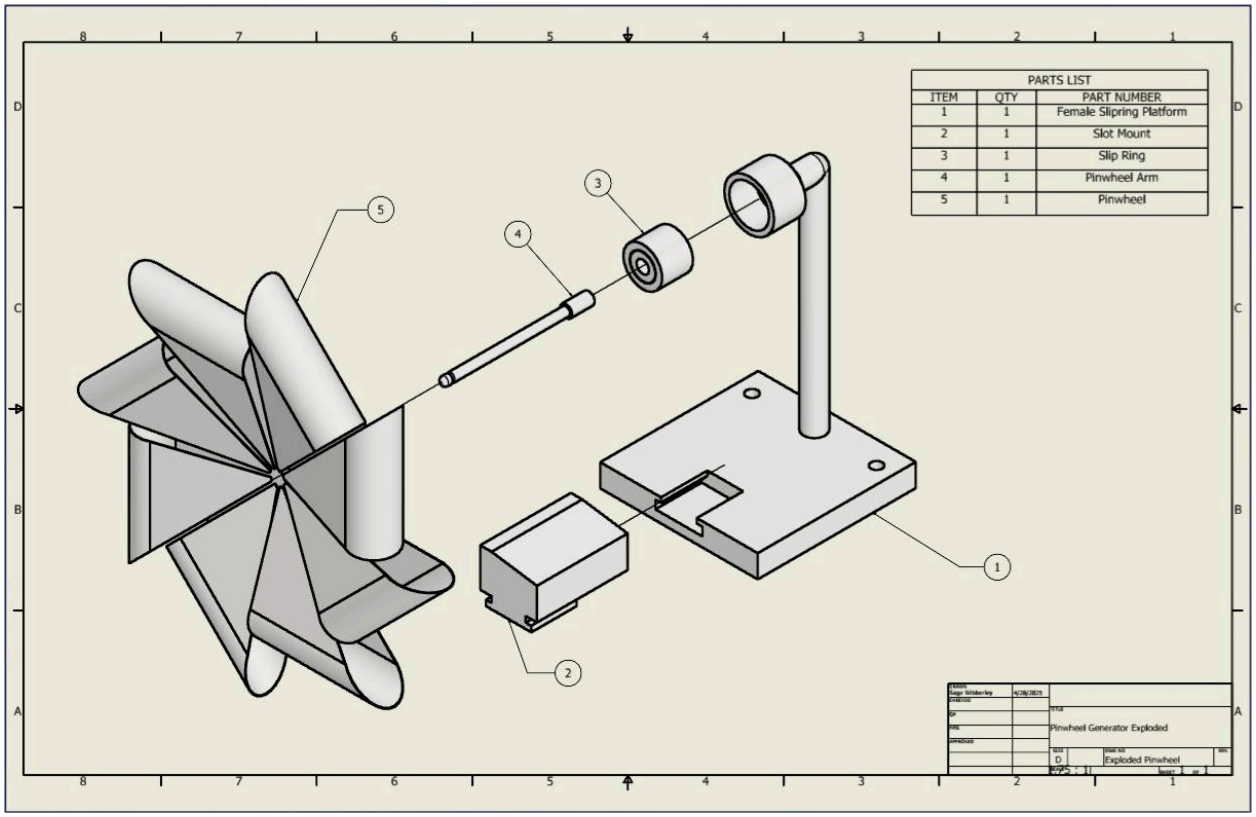

Figure 33: Pinwheel Generator Assembly

The pinwheel generator is composed of five components: a platform, slotted mount, slip ring, pinwheel arm, and pinwheel. The platform houses and positions the other components, and includes two screw holes used to mount the device to the wind tunnel. At the base of this platform, a track allows for different shaped mounts holding a triboelectric material to be installed. Extending from the base is a tightly toleranced mount capable of securing the slip ring. An adhesive then holds the pinwheel arm, with the pinwheel attached, into the other end of the slip ring, which is still capable of rotating freely. Figure 33 displays these parts assembled.

Triboelectricity is generated when a positive triboelectric material attached onto the wing tips contacts a negative triboelectric material placed on the base. The experimental setup used copper on the pinwheel and teflon on the mount. Using the same materials as the leaf design allows for more apt comparison between the generators. Wires from the copper were connected through a slip ring and the teflon from the mount and then attached to the electrical circuit. This setup allows for voltage created by the pinwheel generator to be displayed using an oscilloscope. The results of this can be seen in figure 34 below, which shows voltage spikes at 4 V and a sustained voltage of 40 mV.

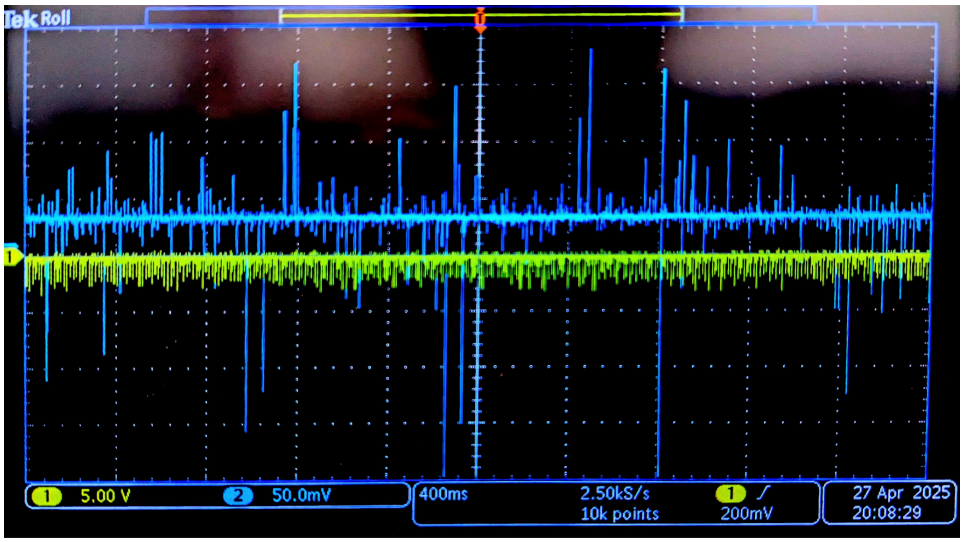

Figure 34: Oscilloscope results of pinwheel generator testing at 19 mph

The generator was tested in wind speeds between 5-20 mph. While capable of generating some voltage at 5 mph, it peaked at a low 5-6 mV at this speed. This increased approximately linearly to the max testing speed of 20 mph, which yielded roughly 40 mV. During testing a handful of flaws became apparent: blade orientation reduced the contact area, the stand experienced more deformation than expected, poor tolerancing of the slip ring reduced pinwheel energy through friction, and high wind speeds caused damage to the teflon pad. The narrow tips of the pinwheel's wings meant that contact area was very small, reducing voltage generated; and this small area and repeated contact at high wind speeds (approaching 20 mph) damaged the teflon used for energy collection. Cyclical deformation of the platform and friction introduced from the slip ring also appeared to siphon energy away from the pinwheel.

The pinwheel generator still offers room for significant improvement. Aligning the wing material parallel to the mount material stands to significantly increase contact area, thus increasing output voltage. Additionally, upgrading the slip ring and reinforcing the platform to limit its mobility could further increase voltage output by reducing energy loss. Upgrading the triboelectric materials offers further improvement. First by increasing resistance to damage from the blade, then by allowing for selection of more triboelectrically opposite materials. Copper and teflon were selected to ensure valid comparison to other designs, but the lack of need for flexibility reveals an array of potential improvements. Selecting stiffer materials with lower friction coefficients and a greater triboelectric polarity stands to increase voltage, durability, and efficiency of the system.

In summary, the pinwheel generator demonstrates a promising development in triboelectric power generation. While the device remains in early development, it serves as a proof of concept for, essentially, scaled down wind turbines. In achieving voltage generation in

low-speed winds (beginning at 5 mph), this generator validates the feasibility of triboelectric charging in low-wind environments. With continued support and concerted effort to raise voltage production, the pinwheel generator can potentially produce noteworthy energy generation.

Summary and Conclusions:

This project focused on designing and creating a triboelectric wind energy harvesting system optimized for low-speed urban wind environments. The main goal was to maximize DC voltage output while maintaining structural reliability across a range of wind speeds. Through an iterative prototyping process with 3D printing TPU as the primary manufacturing method, a flexible leaf-inspired blade system that utilizes triboelectric materials was designed. The triboelectric materials chosen were teflon (negative) and copper (positive) due to their voltage generation during testing in addition to their ease of application. The two triboelectric materials of opposing charges generate electrical power through repeated contact and separation. The system converted the resulting voltage peaks from the contact separation into a constant voltage output using a bridge rectifier and capacitor.

Testing in the wind tunnel revealed promising results. At wind speeds of 19 mph, voltage peaks ranged from 35–60 V with a steady DC output of approximately 100 mV. At 21 mph, peak voltages increased to 50–70 V with a DC output of 120 mV. At 23 mph, voltage peaks reached 60–95 V with a slightly elevated DC output of 130 mV. These results confirm that voltage output scales with wind speeds from six to 30 MPH, which was the range tested, and that the triboelectric design functions as expected in higher wind conditions. In a similar pattern to how voltage and wind speed have a mutual relationship, the leaves would vibrate with a higher frequency as the wind speed increased.

There were several positive takeaways from this project. The leaf-inspired blade design (Figure 21) successfully generated measurable voltage under various wind speeds, showing the effectiveness of using teflon and copper as triboelectric materials for power generation. In addition, flexible TPU was used for rapid prototyping, allowing for refined blade geometries and improving the potential of mechanical deflection with respect to wind flow. Additionally, the electrical system converted the voltage peaks into a mostly steady output. These results confirm the feasibility of triboelectric wind energy generation and validate the material selection and structural design.

Meanwhile, certain limitations to the design still remain, such as the DC voltage output being too low to power a device and the systems efficiency at low wind speeds is limited by insufficient mechanical deflection. The variability in contact pressure and how it results in significant wear on the blades after a few tests as well as the various environmental factors that were not taken into consideration when testing in the wind tunnel can further impact the output consistency. While the DC output was generally smooth, at higher wind speeds more ripples were observed. A variable capacitor and a resistor placed in parallel could be used to further smooth out the resulting voltage.

Furthermore, future work should focus on improving the system at lower wind speeds through exploring alternative geometries or materials with a lower elastic modulus. Determining the fatigue life of the system would be crucial in knowing how long the individual leaves and triboelectric materials can survive. Further testing with an array of leaves is essential to evaluate the collective implementation, possibly resulting in much higher power generation. Incorporating small-scale energy storage and further refining of the electrical circuit could also enhance practical applications. Overall, this project demonstrates the potential for a triboelectric wind

energy system to serve as a sustainable, small-scale, and adaptable solution for energy needs that are ever changing.

Appendix A: References

200 Watt Solar Panel How Many Amps? (2023, October 16). ShopSolar.Com. https://shopsolarkits.com/blogs/learning-center/200-watt-solar-panel-how-many-amps

Advantages and Challenges of Wind Energy. (n.d.). Energy.Gov. Retrieved May 1, 2025, from https://www.energy.gov/eere/wind/advantages-and-challenges-wind-energy

Benson, T. (n.d.). Shape Effects on Drag. NASA. Retrieved November 22, 2024, from https://www.grc.nasa.gov/www/k-12/VirtualAero/BottleRocket/airplane/shaped.html

Bridge Rectifier: Circuit Diagram, Types, Working & Its Applications. (n.d.). ElProCus - Electronic Projects for Engineering Students. Retrieved December 9, 2024, from https://www.elprocus.com/bridge-rectifier-circuit-theory-with-working-operation/

Budynas, R. G. (n.d.). Shigley's Mechanical Engineering Design: 2024 Release (11th ed.). Retrieved December 12, 2024, from https://online.vitalsource.com/reader/books/9781260407679

Cao, D., Song, L., Li, J., Yuan, J., & Zhou, Y. (2014). Determining the drag coefficient of a cylinder perpendicular to water flow by numerical simulation and field measurement. Ocean Engineering, 85, 93–99. https://doi.org/10.1016/j.oceaneng.2014.04.028

Chapman, D. (2016). High Conductivity Copper for Electrical Engineering. Copper Development Association, 122, 14–15.

Cheng, T., Gao, Q., & Wang, Z. L. (2019). The Current Development and Future Outlook of Triboelectric Nanogenerators: A Survey of Literature. Advanced Materials Technologies, 4(3), 1800588. https://doi.org/10.1002/admt.201800588

Forward Bias vs. Reverse Bias and their Effects on Diode Functionality. (2024, August 7). Cadence. https://resources.pcb.cadence.com/blog/2020-forward-bias-vs-reverse-bias-and-their-effects-on-diode-functionality

Gent, A. N. (1958). On the Relation between Indentation Hardness and Young's Modulus. Rubber Chemistry and Technology, 31(4), 896–906. https://doi.org/10.5254/1.3542351

Gross, S. (2020, January). Renewables, land use, and local opposition in the United States. Brookings. https://www.brookings.edu/articles/renewables-land-use-and-local-opposition-in-the-united-states/

Half Wave and Full Wave Rectifier: Function, Comparison, and Applications. (n.d.). ROHM Semiconductor. Retrieved December 6, 2024, from https://www.rohm.com/electronics-basics/ac-dc-converters/acdc_what2

How Do Wind Turbines Survive Severe Weather and Storms? (2024, July 17). Department of Energy. https://www.energy.gov/eere/articles/how-do-wind-turbines-survive-severe-weather-and-storms

International Standard Atmosphere. (n.d.). Engineering Toolbox. Retrieved November 22, 2024, from https://www.engineeringtoolbox.com/international-standard-atmosphere-d_985.html

Lacks, D. J., & Shinbrot, T. (2019). Long-standing and unresolved issues in triboelectric charging. Nature Reviews Chemistry, 3(8), 465–476. https://doi.org/10.1038/s41570-019-0115-1

Liu, S., Zheng, W., Yang, B., & Tao, X. (2018). Triboelectric charge density of porous and deformable fabrics made from polymer fibers. Nano Energy, 53, 383–390. https://doi.org/10.1016/j.nanoen.2018.08.071

Merino, D. (2020, July 23). The first undeniable climate change deaths: Japan's 2018 heat wave. Slate. https://slate.com/technology/2020/07/climate-change-deaths-japan-2018-heat-wave.html

Radi, A., Thompson, M. C., Sheridan, J., & Hourigan, K. (2013). From the circular cylinder to the flat plate wake: The variation of Strouhal number with Reynolds number for elliptical cylinders. Physics of Fluids, 25(10), 101706. https://doi.org/10.1063/1.4827521

Rostami, A. B., Mobasheramini, M., & Fernandes, A. C. (2019). Strouhal number of flat and flapped plates at moderate Reynolds number and different angles of attack: Experimental data. Acta Mechanica, 230(1), 333–349. https://doi.org/10.1007/s00707-018-2292-2

Sabins, D. (2024, November 6). The Cost of Going Solar | SaveOnEnergy. SaveOnEnergy.Com. https://www.saveonenergy.com/solar-energy/solar-cost-over-time/

Storr, W. (2013, August 13). Full Wave Rectifier and Bridge Rectifier Theory. Basic Electronics Tutorials. https://www.electronics-tutorials.ws/diode/diode_6.html

Triboelectricity. (n.d.). MRSEC Education Group. Retrieved April 28, 2025, from https://education.mrsec.wisc.edu/triboelectricity/

UltiMaker. (n.d.). Technical data sheet TPU 95A. Retrieved May 2, 2025, from https://www.matterhackers.com/r/0HMNp5

US Department of Commerce, N. (n.d.). Wind Threat Defined. National Weather Service; NOAA's National Weather Service. Retrieved November 22, 2024, from https://www.weather.gov/mlb/wind_threat

What is U.S. electricity generation by energy source? (n.d.). EIA. Retrieved April 28, 2025, from https://www.eia.gov/tools/faqs/faq.php?id=427&t=3

Wilson, A. (2009, April 29). The Folly of Building-Integrated Wind. BuildingGreen. https://www.buildinggreen.com/feature/folly-building-integrated-wind

WINDExchange: Virginia 30-Meter Residential-Scale Wind Resource Map. (n.d.). Retrieved April 24, 2025, from https://windexchange.energy.gov/maps-data/239

Wu, C., Wang, A. C., Ding, W., Guo, H., & Wang, Z. L. (2019). Triboelectric Nanogenerator: A Foundation of the Energy for the New Era. Advanced Energy Materials, 9(1), 1802906. https://doi.org/10.1002/aenm.201802906

Xu, C., Zi, Y., Wang, A. C., Zou, H., Dai, Y., He, X., Wang, P., Wang, Y., Feng, P., Li, D., & Wang, Z. L. (2018). On the Electron‐Transfer Mechanism in the Contact‐Electrification Effect. Advanced Materials, 30(15), 1706790. https://doi.org/10.1002/adma.201706790

Zou, H., Zhang, Y., Guo, L., Wang, P., He, X., Dai, G., Zheng, H., Chen, C., Wang, A. C., Xu, C., & Wang, Z. L. (2019). Quantifying the triboelectric series. Nature Communications, 10(1), 1427. https://doi.org/10.1038/s41467-019-09461-x

Appendix B: Prototype Design

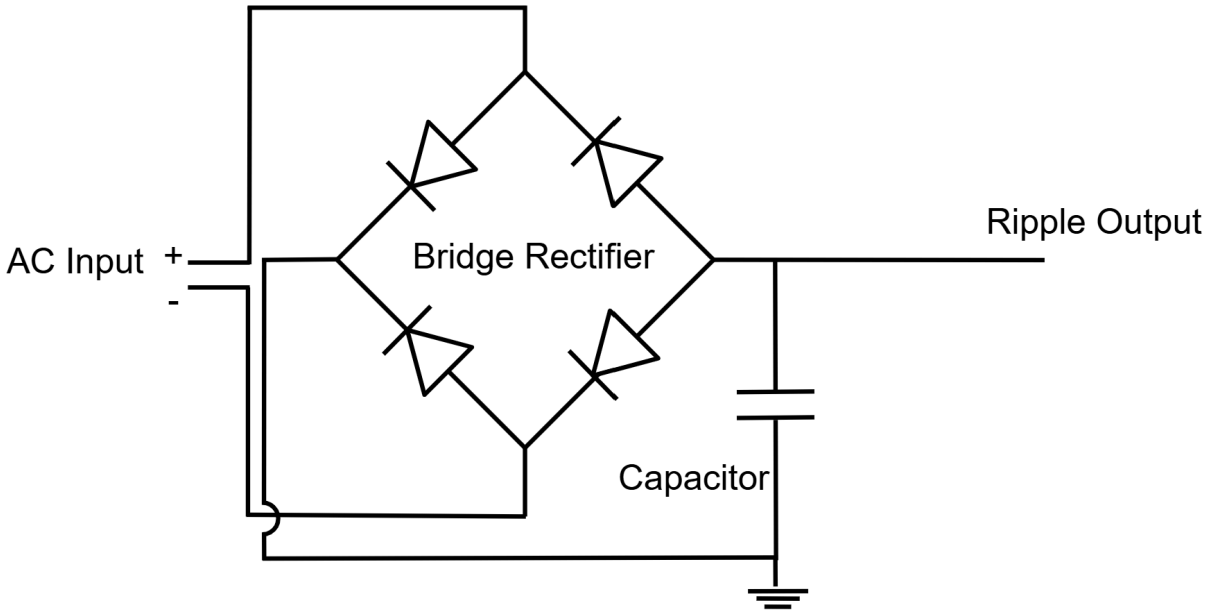

Figure 1: AC to DC converter electrical circuit

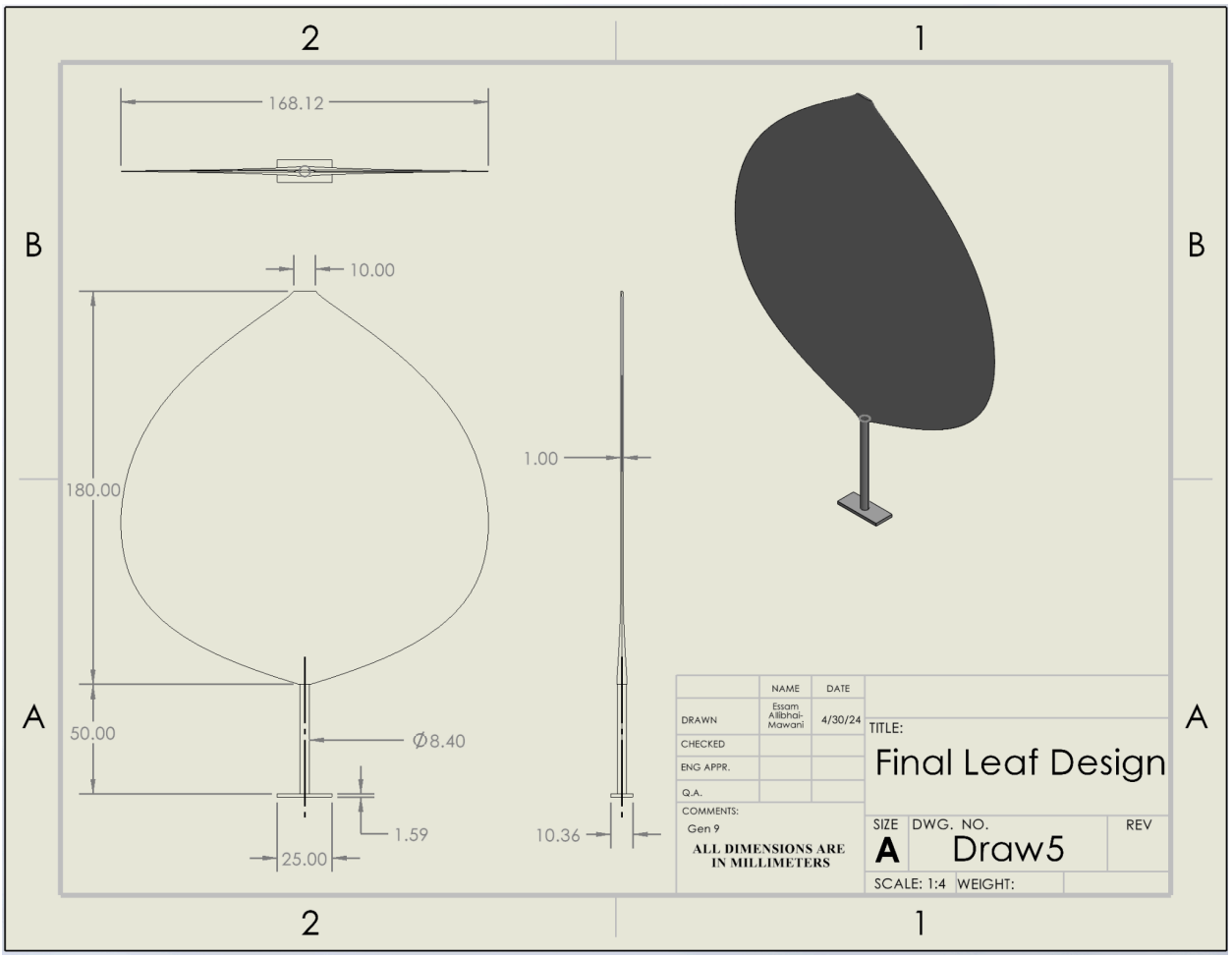

Figure 2: Final Leaf Design

Appendix C: Alternative Designs

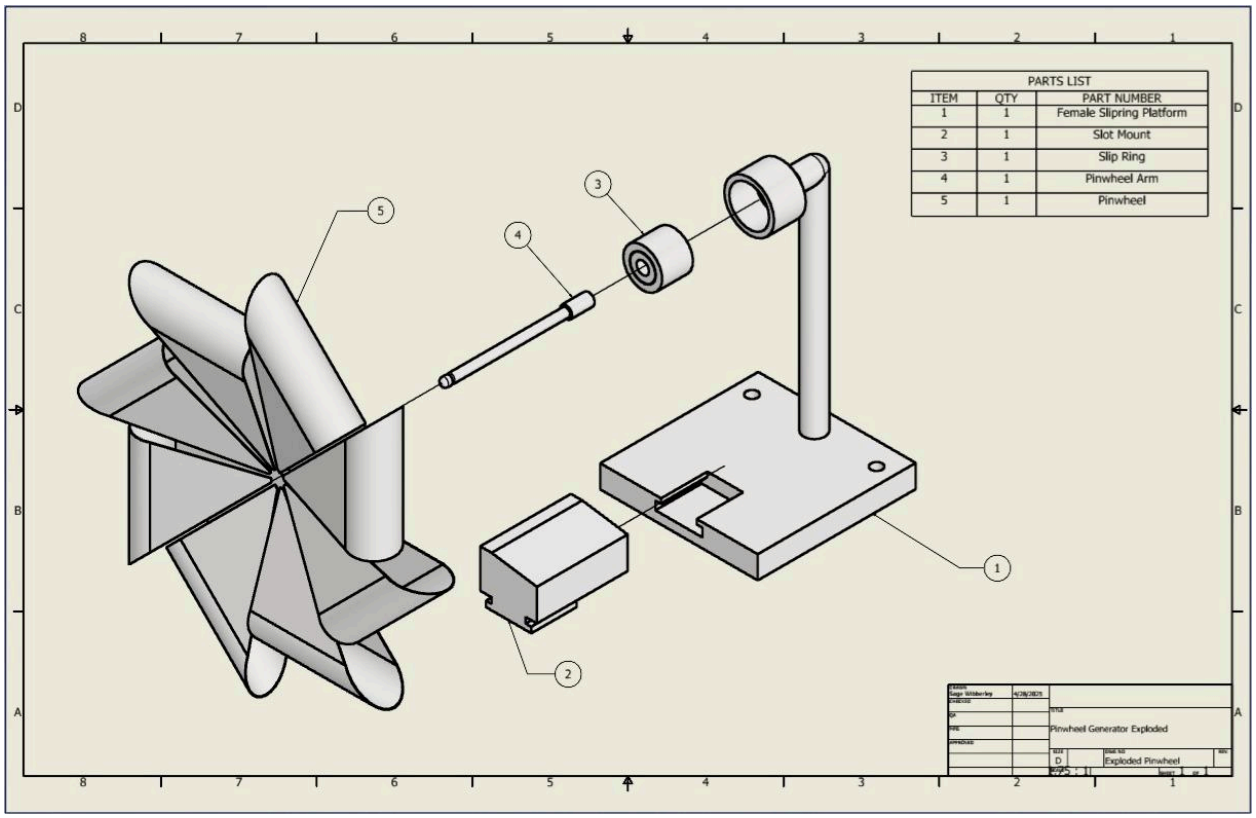

Figure 1: Alternative Pinwheel Design

Appendix D: Reaction forces and deflection calculations a cylindrical blade design

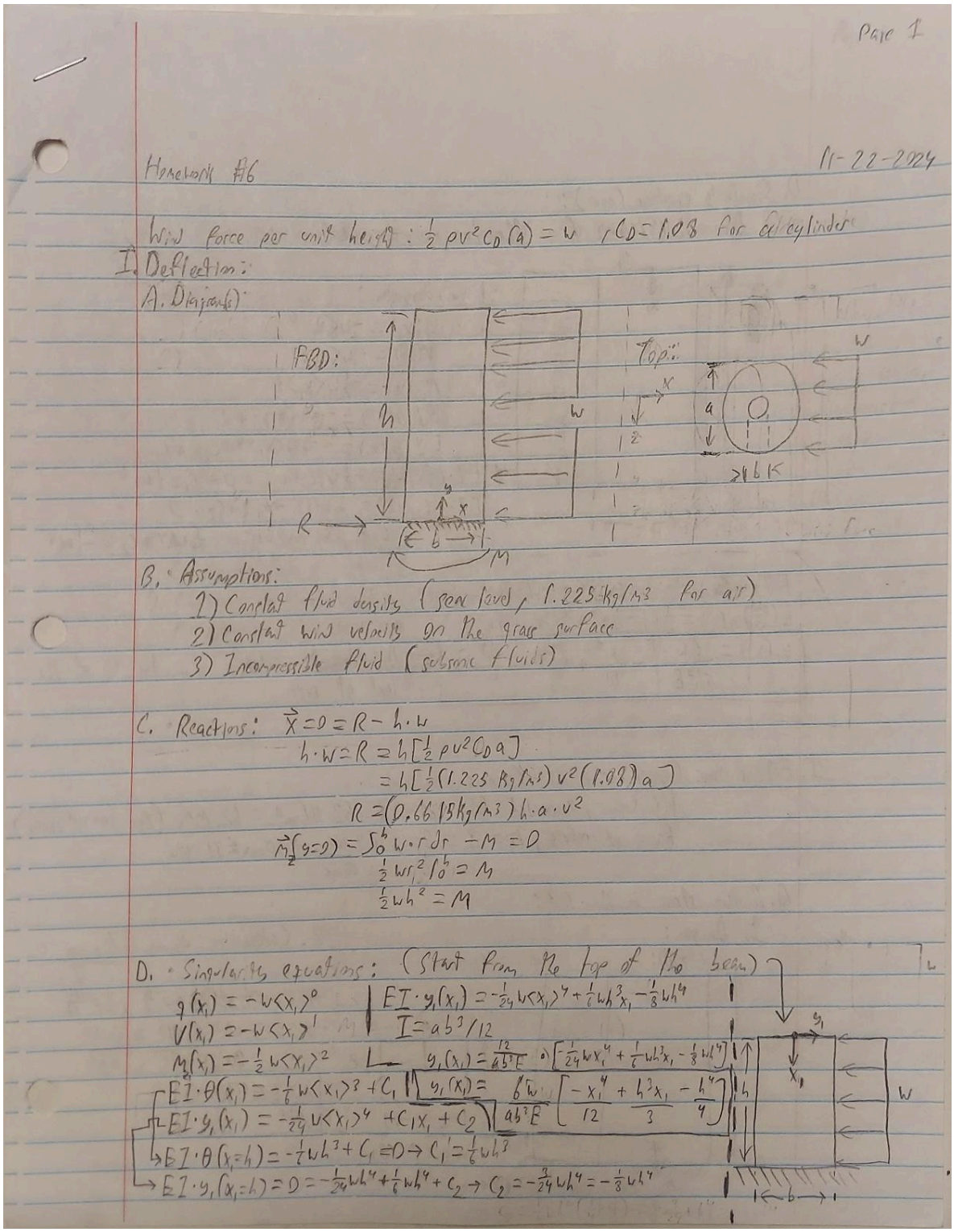

D. Singularity equations (neat):

2. Diagram: (Starting from the top so the reactions can be ignored)

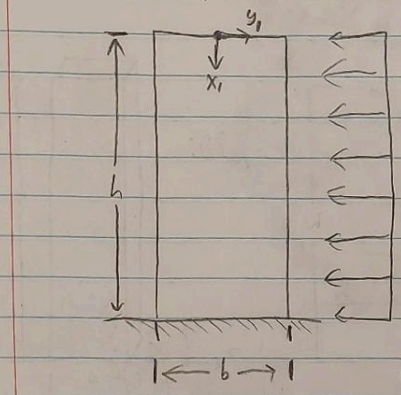

2. Derivation:

$q(x_1) = -w\langle x_1\rangle^0$

$V(x_1) = -w\langle x_1\rangle^1$

$M_{z_1}(x_1) = -\frac{1}{2}w\langle x_1\rangle^2$

$EI\cdot\theta(x_1) = -\frac{1}{6}w\langle x_1\rangle^3 + C_1$

$EI\cdot y_1(x_1) = -\frac{1}{24}w\langle x_1\rangle^4 + C_1x_1 + C_2$

$EI\cdot\theta(x_1=h) = -\frac{1}{6}w(l)^3 + C_1 = 0 \rightarrow C_1 = \frac{1}{6}wh^3$

$EI\cdot y_1(x_1=h) = -\frac{1}{24}w(h)^4 + C_1\cdot h + C_2 = 0$

$C_2 = \frac{1}{24}wh^4 - \frac{1}{6}wh^4 = -\frac{3}{24}wh^4 \rightarrow C_2 = -\frac{1}{8}wh^4$

$EI\cdot y_1(x_1) = -\frac{1}{24}w(x_1)^4 + \frac{1}{6}wh^3(x_1) - \frac{1}{8}wh^4$, $I = ab^3/12$

$E\left(\frac{ab^3}{12}\right)y_1(x_1) = \frac{1}{2}w\left[-\frac{1}{12}x_1^4 + \frac{1}{3}h^3x_1 - \frac{1}{4}h^4\right]$

$$y_1(x_1) = \frac{6w}{ab^3E}\left[-\frac{x_1^4}{12} + \frac{h^3x_1}{3} - \frac{h^4}{4}\right]$$

← Displacement relative to the tip of the leaf at rest

Appendix E: Dimensions of the Flat Blade Prototypes

Table 1

Dimensions of the Flat Blade Prototypes

Height (cm)	Thickness (mm)			
	1.2	1.6	2	2.4
First Batch of Blade Prototypes				
15.24	Blade A1	Blade B1	Blade C1	Blade D1
Second Batch of Blade Prototypes				
7.62	Blade A2	Blade B2	Blade C2	Blade D2
7.874	Blade A3	Blade B3	Blade C3	Blade D3
8.128	Blade A4	Blade B4	Blade C4	Blade D4
Third Batch of Blade Prototypes				
11.938	Blade A5	Blade B5	Blade C5	Blade D5
12.192	Blade A6	Blade B6	Blade C6	Blade D6
12.446	Blade A7	Blade B7	Blade C7	Blade D7

Appendix F: MATLAB Code: Geometric optimization; preliminary calculations

```
%GLOBALS
   rho = 1.225; %Air Density (Kg/m^3)
   v = 4.47; %Inflow velocity (m/s; converted from 10 mph)
   %v = linspace(0,10);
   E = 12000000; %Elastic modulus of TPE83A (Pa)
   x = 0; %poisition were measuring from[0 is the tip of the stem]
   rho_TPE = 1190; %density of TPE83A (kg/m^3;)
 %leaf---------------------------------------------------------------
   C_D_leaf = 1.17; %coefficient of drag of a cylindrical plate
       r_leaf = 0.05; %radius of the leaf face (m; converted from 30 mm)
       %r_leaf = linspace(0.001,0.1);
       t_leaf = 0.001; %thickness of leaf (m; converted from 3mm)
       h_leaf = 0.14; %2*r_leaf; %height of the leaf face (took 0.06 from
current leaf face)
       A_leaf = pi * r_leaf * h_leaf * 0.5; %m^2
 %rectangle x-sec-----------------------------------------------------
   C_D_rect = 1.28; %coefficient of drag of a flat plate
       h_rect = 0.035; %height of the rectangular prisim (m; 35mm)
       w = 0.003; %width of the rectangle (m; 3mm)
       t = 0.001; %thickness of the rectangle (m; 1mm)
       t_i = 0.0005; %inner thickness of a hollow rectangle (m; 0.5 mm)
 %circular x-sec------------------------------------------------------
   C_D_circ = 1.08; %coefficient of drag of the cylinder
       h_circ = 0.06; %height of the cylinder (m; converted from 35mm)
       d = 0.0034; %diameter of the circle (m; converted from 3 mm)
       d_o = 0.003; %outer diameter of the hollow circle (m; 3mm)
       d_i = 0.002; %inner diameter of the hollow circle (m; 2mm)

%FORCES
  % P = 0.5 * rho * v.^2 * C_D_leaf * pi * r_leaf.^2; %point load on tip of
cylinder due to leaf drag force
   P = 0.5 * rho * v.^2 * C_D_leaf * A_leaf %point load on tip of cylinder due
to leaf drag force
   W_rect = 0.5 * rho * v.^2 * C_D_rect * h_rect * w; %distributed load on stem
due to drag force
```

```
   W_circ = 0.5 * rho * v.^2 * C_D_circ * h_circ * d %distributed load on stem
due to drag force
%INERTIAS
   I_rect_whole = (t*w.^3)/12;
   I_rect_hollow = ((t*w.^3)-(t-(2*t_i))*(w-(2*t)).^3)/12;
   I_circ_whole = (pi * d.^4)/64;
   I_circ_hollow = (pi * (d_o.^4 - d_i.^4))/64;
%ANGLE OF DISPLACEMENT
   theta_rect = -((P/(2*E*I_rect_whole))*(x.^2 - h_rect.^2)) +
((W_rect/(6*E*I_rect_whole))*(x.^3 - h_rect.^3));
   theta_rect_hollow = -((P/(2*E*I_rect_hollow))*(x.^2 - h_rect.^2)) +
((W_rect/(6*E*I_rect_hollow))*(x.^3 - h_rect.^3));
   theta_circ = -((P/(2*E*I_circ_whole))*(x.^2 - h_circ.^2)) +
((W_circ/(6*E*I_circ_whole))*(x.^3 - h_circ.^3));
   theta_circ_hollow = -((P/(2*E*I_circ_hollow))*(x.^2 - h_circ.^2)) +
((W_circ/(6*E*I_circ_hollow))*(x.^3 - h_circ.^3));
%STEM DISPLACEMENT
   delta_rect =
((P/(6*E*I_rect_whole))*((x.^3)-((3)*(h_rect.^2)*(x))+((2)*(h_rect.^3)))) +
((W_rect/(24*E*I_rect_whole))*((x.^4)-((4)*(h_rect.^3)*(x))+((3)*(h_rect.^4))))
;
   delta_rect_hollow =
((P/(6*E*I_rect_hollow))*((x.^3)-((3)*(h_rect.^2)*(x))+((2)*(h_rect.^3)))) +
((W_rect/(24*E*I_rect_hollow))*((x.^4)-((4)*(h_rect.^3)*(x))+((3)*(h_rect.^4)))
);
   delta_circ =
((P/(6*E*I_circ_whole))*((x.^3)-((3)*(h_circ.^2)*(x))+((2)*(h_circ.^3)))) +
((W_circ/(24*E*I_circ_whole))*((x.^4)-((4)*(h_circ.^3)*(x))+((3)*(h_circ.^4))))
;
   delta_circ_hollow =
((P/(6*E*I_circ_hollow))*((x.^3)-((3)*(h_circ.^2)*(x))+((2)*(h_circ.^3)))) +
((W_circ/(24*E*I_circ_hollow))*((x.^4)-((4)*(h_circ.^3)*(x))+((3)*(h_circ.^4)))
);
%TIP DISPLACEMENT
   disp_rect_tip = delta_rect + sin(theta_rect)*h_leaf;
   disp_rect_tip_hollow = delta_rect_hollow + sin(theta_rect_hollow)*h_leaf;
   disp_circ_tip = delta_circ + sin(theta_circ)*h_leaf
   disp_circ_tip_hollow = delta_circ_hollow + sin(theta_circ_hollow)*h_leaf;
```

```
%NATURAL FREQUENCY
   V_mass = A_leaf * t_leaf;
   m_mass = V_mass * rho_TPE;
   l_mass = (h_leaf/2) + h_circ;
   %full circle
   V_beam_circ = pi * d.^2 * h_circ;
   m_beam_circ = V_beam_circ * rho_TPE;
   Freq_n_circ = (1/(2*pi))*(sqrt(3*E*I_circ_whole) /
(((0.2235*m_beam_circ)+(m_mass))*(l_mass.^3)))
   %hollow circle
   V_beam_circ_hollow = pi * h_circ * 0.25 * ((d_o.^2)-(d_i.^2));
   m_beam_circ_hollow = V_beam_circ_hollow * rho_TPE;
   Freq_n_circ_hollow = (1/(2*pi))*(sqrt(3*E*I_circ_hollow)) /
(((0.2235*m_beam_circ_hollow)+(m_mass))*(l_mass.^3));
   %whole rectangle
   V_beam_rect = w * t * h_rect;
   m_beam_rect = V_beam_rect * rho_TPE;
   Freq_n_rect = (1/(2*pi))*(sqrt(3*E*I_rect_whole)) /
(((0.2235*m_beam_rect)+(m_mass))*(l_mass.^3));
   %hollow rectangle
   V_beam_rect_hollow = 2 * h_rect * (w + t - 2);
   m_beam_rect_hollow = V_beam_rect_hollow * rho_TPE;
   Freq_n_rect_hollow = (1/(2*pi))*(sqrt(3*E*I_rect_hollow)) /
(((0.2235*m_beam_rect_hollow)+(m_mass))*(l_mass.^3));
%BENDING STRESS
   Sig_xx_circ = (((P*h_circ)+(((W_circ)*(h_circ.^2))/2))*(d/2))/I_circ_whole;
   Sig_xx_circ_hollow =
(((P*h_circ)+(((W_circ)*(h_circ.^2))/2))*(d/2))/I_circ_hollow;
   Sig_xx_rect = (((P*h_rect)+(((W_rect)*(h_rect.^2))/2))*(w/2))/I_rect_whole;
   Sig_xx_rect_hollow =
(((P*h_rect)+(((W_rect)*(h_rect.^2))/2))*(w/2))/I_rect_hollow;
%BUCKLING
   L_leaf = m_mass * 9.81;
   L_crit_circ = (pi.^2 * E * I_circ_whole)/(4*h_circ.^2);
   L_crit_circ_hollow = (pi.^2 * E * I_circ_hollow)/(4*h_circ.^2);
   L_crit_rect = (pi.^2 * E * I_rect_whole)/(4*h_rect.^2);
   L_crit_rect_hollow = (pi.^2 * E * I_rect_hollow)/(4*h_rect.^2);
```

Appendix G: MATLAB Code Geometric Optimization; final iteration

```
function findOptimalDesign6()
   % Display header
   fprintf('================================================\n');
   fprintf('FINDING CONFIGURATION WITH OPTIMAL DESIGN\n');
   fprintf('Maximizing leaf area with targeted displacement and enhanced
buckling safety\n');
   fprintf('All constraints are enforced: \n');
   fprintf('  - Height < 0.25m\n');
   fprintf('  - Stress within limits\n');
   fprintf('  - Displacement ~95%% of maximum allowable\n');
   fprintf('  - Critical buckling load > 1.5x applied load\n');
   fprintf('================================================\n\n');

   % Define parameter space
   r_leaf_values = 0.005:0.001:0.08;  % Finer increments for radius
   t_leaf_values = 0.001:0.0005:0.03; % Finer increments for thickness
   h_leaf_values = 0.02:0.005:0.18;   % Finer increments for height
   h_circ_values = 0.02:0.005:0.18;   % Finer increments for circular section
height
   d_values = 0.002:0.0002:0.01;     % Finer increments for diameter

   % Define weights for multi-objective function
   w_area = 0.5;        % Weight for leaf area
   w_displacement = 0.5; % Weight for displacement (targeting 95% of allowable)

   % Target displacement ratio (95% of allowable)
   targetDisplacementRatio = 0.95;

   % Initialize tracking for maximum combined score
   maxCombinedScore = 0;
   bestConfig = [];

   % Search all valid configurations
   fprintf('Searching for configuration with optimal balance of leaf area and
displacement...\n');

   totalConfigs = length(r_leaf_values) * length(t_leaf_values) *
length(h_leaf_values) * ...
                  length(h_circ_values) * length(d_values);
   fprintf('Total configurations to check: %d\n', totalConfigs);

   configsChecked = 0;
   validConfigs = 0;

   % Setup progress reporting
   progressStep = floor(totalConfigs / 10);
   nextProgressReport = progressStep;

   for r = r_leaf_values
       for t = t_leaf_values
           for h = h_leaf_values
               for hc = h_circ_values
                   % Skip if total height exceeds 0.25
                   if h + hc > 0.25
```

```
                    continue;
                end

                for diam = d_values
                    configsChecked = configsChecked + 1;

                    % Progress reporting
                    if configsChecked >= nextProgressReport
                        fprintf('Progress: %.1f%% complete (%d
configurations checked, %d valid so far)\n', ...
                            (configsChecked/totalConfigs)*100,
configsChecked, validConfigs);
                        nextProgressReport = nextProgressReport +
progressStep;
                    end

                    [constraints, results] = evaluateConstraints(r, t, h,
hc, diam);

                    % Add enhanced buckling safety constraint
                    bucklingConstraint = results.L_crit_circ > (1.5 *
results.L_leaf);

                    if all(constraints) && bucklingConstraint
                        validConfigs = validConfigs + 1;

                        % Calculate leaf area (ovular plate)
                        leafArea = pi * r * h * 0.5;

                        % Calculate displacement ratio (higher is better, up
to allowable limit)
                        displacementRatio = results.disp_circ_tip / (h +
hc);

                        % Calculate normalized scores (0 to 1)
                        % For area: normalize against theoretical maximum
area (r=0.08, h = 0.18)
                        maxPossibleArea = pi * 0.08 * 0.18 *0.5;
                        normalizedAreaScore = leafArea / maxPossibleArea;

                        % For displacement: we want to get as close as
possible to 95% of allowable
                        % Score is based on how close we are to the target
(95%)
                        displacementScore = 1 - abs(displacementRatio -
targetDisplacementRatio);

                        % Compute combined score using weighted sum
                        combinedScore = (w_area * normalizedAreaScore) +
(w_displacement * displacementScore);

                        % If this configuration has a higher combined score
than previous best
                        if combinedScore > maxCombinedScore
                            maxCombinedScore = combinedScore;
                            bestConfig = struct(...
                                'r_leaf', r, ...
```

```
                                    't_leaf', t, ...
                                    'h_leaf', h, ...
                                    'h_circ', hc, ...
                                    'd', diam, ...
                                    'leaf_area', leafArea, ...
                                    'disp_circ_tip', results.disp_circ_tip, ...
                                    'total_height', h + hc, ...
                                    'displacement_ratio', displacementRatio *
100, ... % as percentage
                                    'normalized_area_score',
normalizedAreaScore, ...
                                    'displacement_score', displacementScore, ...
                                    'combined_score', combinedScore, ...
                                    'Sig_xx_circ', results.Sig_xx_circ, ...
                                    'L_leaf', results.L_leaf, ...
                                    'L_crit_circ', results.L_crit_circ, ...
                                    'buckling_safety_factor',
results.L_crit_circ / results.L_leaf ...
                                );
                            end
                        end
                    end
                end
            end
        end
    end

    % Display results
    fprintf('\n================================================\n');
    fprintf('OPTIMAL CONFIGURATION WITH ENHANCED CONSTRAINTS\n');
    fprintf('================================================\n');

    if ~isempty(bestConfig)
        fprintf('Geometric Parameters:\n');
        fprintf('  r_leaf: %.4f m\n', bestConfig.r_leaf);
        fprintf('  t_leaf: %.4f m\n', bestConfig.t_leaf);
        fprintf('  h_leaf: %.4f m\n', bestConfig.h_leaf);
        fprintf('  h_circ: %.4f m\n', bestConfig.h_circ);
        fprintf('  d: %.4f m\n', bestConfig.d);
        fprintf('  Total height: %.4f m\n', bestConfig.total_height);

        fprintf('\nPerformance Metrics:\n');
        fprintf('  Leaf Area: %.6f m²\n', bestConfig.leaf_area);
        fprintf('  Displacement: %.4e m (%.1f%% of allowable limit)\n', ...
            bestConfig.disp_circ_tip, bestConfig.displacement_ratio);
        fprintf('  Target displacement: 95.0%% of allowable\n');
        fprintf('  Combined optimization score: %.4f\n',
bestConfig.combined_score);
        fprintf('  (Area score: %.4f, Displacement proximity score: %.4f)\n',
...
            bestConfig.normalized_area_score, bestConfig.displacement_score);
        fprintf('  Allowable displacement limit: %.4e m\n',
bestConfig.total_height);
        fprintf('  Bending stress: %.1.5e Pa (limit: %.1.5e Pa)\n', ...
            bestConfig.Sig_xx_circ, 3.2e7);
        fprintf('  Buckling: Leaf load=%.4f N, Critical load=%.4e N\n', ...
            bestConfig.L_leaf, bestConfig.L_crit_circ);
```

```
        fprintf('  Buckling safety factor: %.2f (> 1.5 required)\n', ...
            bestConfig.buckling_safety_factor);
    else
        fprintf('No valid configuration found.\n');
    end

    % Also find multiple configurations with high combined scores
    fprintf('\n================================================\n');
    fprintf('MULTIPLE HIGH PERFORMANCE CONFIGURATIONS\n');
    fprintf('================================================\n');

    % We'll track top 10 configurations with highest combined scores
    topConfigs = [];
    numTopConfigs = 10;

    for r = r_leaf_values
        for t = t_leaf_values
            for h = h_leaf_values
                for hc = h_circ_values
                    % Skip if total height exceeds 0.25
                    if h + hc > 0.25
                        continue;
                    end

                    for diam = d_values
                        [constraints, results] = evaluateConstraints(r, t, h,
hc, diam);

                        % Add enhanced buckling safety constraint
                        bucklingConstraint = results.L_crit_circ > (1.5 *
results.L_leaf);

                        if all(constraints) && bucklingConstraint
                            % Calculate leaf area
                            leafArea = pi * r * h * 0.5;

                            % Calculate displacement ratio
                            displacementRatio = results.disp_circ_tip / (h +
hc);

                            % Calculate normalized scores
                            maxPossibleArea = pi * 0.08 * 0.18 * 0.5;
                            normalizedAreaScore = leafArea / maxPossibleArea;
                            displacementScore = 1 - abs(displacementRatio -
targetDisplacementRatio);

                            % Compute combined score
                            combinedScore = (w_area * normalizedAreaScore) +
(w_displacement * displacementScore);

                            config = struct(...
                                'r_leaf', r, ...
                                't_leaf', t, ...
                                'h_leaf', h, ...
                                'h_circ', hc, ...
                                'd', diam, ...
                                'leaf_area', leafArea, ...
```

```
                                'disp_circ_tip', results.disp_circ_tip, ...
                                'total_height', h + hc, ...
                                'displacement_ratio', displacementRatio * 100,
...
                                'normalized_area_score', normalizedAreaScore,
...
                                'displacement_score', displacementScore, ...
                                'combined_score', combinedScore, ...
                                'Sig_xx_circ', results.Sig_xx_circ, ...
                                'L_leaf', results.L_leaf, ...
                                'L_crit_circ', results.L_crit_circ, ...
                                'buckling_safety_factor', results.L_crit_circ /
results.L_leaf ...
                            );

                            % Add to list if it's the first one or has higher
combined score than the smallest in the list
                            if isempty(topConfigs) || length(topConfigs) <
numTopConfigs
                                topConfigs = [topConfigs; config];
                                % Sort by combined score (descending)
                                if length(topConfigs) > 1
                                    [~, idx] = sort([topConfigs.combined_score],
'descend');
                                    topConfigs = topConfigs(idx);
                                end
                            elseif combinedScore >
topConfigs(end).combined_score
                                % Replace the smallest score in our top list
                                topConfigs(end) = config;
                                % Re-sort
                                [~, idx] = sort([topConfigs.combined_score],
'descend');
                                topConfigs = topConfigs(idx);
                            end
                        end
                    end
                end
            end
        end
    end

    if ~isempty(topConfigs)
        fprintf('Top %d configurations with highest combined scores:\n\n',
length(topConfigs));

        for i = 1:length(topConfigs)
            config = topConfigs(i);
            fprintf('Configuration %d (Combined Score: %.4f):\n', i,
config.combined_score);
            fprintf('  r_leaf=%.4fm, t_leaf=%.4fm, h_leaf=%.2fm, h_circ=%.2fm,
d=%.4fm\n', ...
                config.r_leaf, config.t_leaf, config.h_leaf, config.h_circ,
config.d);
            fprintf('  Area: %.6f m², Displacement: %.4e m (%.1f%% of
allowable)\n', ...
```

```
                config.leaf_area, config.disp_circ_tip,
config.displacement_ratio);
            fprintf('  Area score: %.4f, Displacement proximity score: %.4f\n',
...
                config.normalized_area_score, config.displacement_score);
            fprintf('  Buckling safety factor: %.2f\n\n', ...
                config.buckling_safety_factor);
        end
    else
        fprintf('No valid configurations found.\n');
    end
end
% Function to evaluate constraints based on the 5 geometric variables
function [constraints, results] = evaluateConstraints(r_leaf, t_leaf, h_leaf,
h_circ, d)
    % GLOBALS
    rho = 1.225; % Air Density (Kg/m^3)
    v = 4.47; % Inflow velocity (m/s)
    E = 26000000; % Elastic modulus of Ninjatek TPE83A (Pa)
    x = 0; % position we're measuring from [0 is the tip of the stem]
    rho_TPE = 1140; % density of TPE83A (kg/m^3)
    sig_xx_max = 3.9e7;
    g = 9.81; % gravity
    % Leaf parameters
    C_D_leaf = 1.17; % coefficient of drag of a cylindrical plate

    % Circular x-section parameters
    C_D_circ = 1.08; % coefficient of drag of the cylinder

    % FORCES
    P = 0.5 .* rho .* v.^2 .* C_D_leaf .* pi .* r_leaf.* h_leaf * 0.5; % point
load on tip
    W_circ = 0.5 .* rho .* v.^2 .* C_D_circ .* h_circ .* d; % distributed load
on stem

    % INERTIAS
    I_circ_whole = (pi .* (d.^4))./64;

    % ANGLE OF DISPLACEMENT
    theta_circ = -((P ./ (2.*E .* I_circ_whole)) .* (x.^2 - h_circ.^2)) + ...
                 ((W_circ./(6.*E.*I_circ_whole)).*(x.^3 - h_circ.^3));

    % STEM DISPLACEMENT
    delta_circ = ((P ./ (6.*E .* I_circ_whole))
.*((x.^3)-((3).*(h_circ.^2).*(x))+((2).*(h_circ.^3)))) + ...

((W_circ./(24.*E.*I_circ_whole)).*((x.^4)-((4).*(h_circ.^3).*(x))+((3).*(h_circ
.^4))));

    % TIP DISPLACEMENT
    disp_circ_tip = delta_circ + sin(theta_circ).*h_leaf;

    % NATURAL FREQUENCY
    V_mass = (0.5 .* pi .* r_leaf .* (t_leaf) .* (h_leaf));        %change 't'
to consider other matl's
    m_mass = V_mass .* rho_TPE;
    l_mass = (h_leaf./2) + h_circ;
```

```
    % Full circle
    V_beam_circ = pi .* d.^2 .* h_circ;
    m_beam_circ = V_beam_circ .* rho_TPE;
    Freq_n_circ = (1./(2.*pi)).*(sqrt(3.*E.*I_circ_whole)) ./ ...
                  (((0.2235.*m_beam_circ)+(m_mass)).*(l_mass.^3));

    % BENDING STRESS
    Sig_xx_circ = (((P .* h_circ) + ((W_circ .* (h_circ.^2)) ./ 2)) .* (d ./ 2))
./ I_circ_whole;

    % BUCKLING
    L_leaf = m_mass .* g;
    L_crit_circ = (pi.^2 .* E .* I_circ_whole) ./ (4 .* h_circ.^2);

    % Original constraints
    constraint1 = Sig_xx_circ < sig_xx_max; % Bending stress constraint
    constraint2 = disp_circ_tip < (h_circ + h_leaf); % Displacement constraint
    constraint3 = L_leaf < L_crit_circ; % Buckling constraint

    % New constraint: total height < 0.25 m
    constraint4 = (h_circ + h_leaf) < 0.25;

    % Return constraints and detailed results
    constraints = [constraint1, constraint2, constraint3, constraint4];
    results = struct('Sig_xx_circ', Sig_xx_circ, ...
                     'disp_circ_tip', disp_circ_tip, ...
                     'L_leaf', L_leaf, ...
                     'L_crit_circ', L_crit_circ, ...
                     'total_height', h_circ + h_leaf);
end
```

Appendix H: MATLAB Code: Frequency Analysis

```
function videoread()
   % Read video
   mov = VideoReader("C:\Users\gosis\Desktop\Capstone\4-23\IMG_1948.MOV");
   frameRate = mov.FrameRate;
   numFrames = mov.NumberOfFrames;

   % Display first frame for ROI selection
   first_frame = read(mov, 1);
   figure(1), imshow(first_frame);
   title('Select region of interest (2 points for diagonal corners)');

   % Get ROI from user
   [x, y] = ginput(2);
   x1 = round(min(x)); % top left corner
   y1 = round(min(y)); % top left corner
   x2 = round(max(x)); % bottom right corner
   y2 = round(max(y)); % bottom right corner

   % Initialize arrays to store object positions
   positions = zeros(numFrames, 2);
   timePoints = zeros(numFrames, 1);

   % Process each frame - using basic image processing
   for k = 1:numFrames
       % Read frame
       frame = read(mov, k);

       % Extract ROI
       roi = frame(y1:y2, x1:x2, :);

       % Convert to grayscale without using rgb2gray
       if size(roi, 3) > 1
           % Manual grayscale conversion using luminance formula
           roi_gray = 0.2989 * double(roi(:,:,1)) + 0.5870 * double(roi(:,:,2))
+ 0.1140 * double(roi(:,:,3));
           roi_gray = uint8(roi_gray);
       else
           roi_gray = roi;
       end

       % Simple thresholding without using imbinarize
       % Fixed threshold (adjust as needed for your video)
       fixed_thresh = 128;
       bw = roi_gray > fixed_thresh;

       % Find approximate centroid without regionprops
       [rows, cols] = find(bw);
       if ~isempty(rows) && ~isempty(cols)
           centroid_y = mean(rows);
           centroid_x = mean(cols);
           positions(k, 1) = centroid_x;
           positions(k, 2) = centroid_y;
       elseif k > 1
           % Use previous position if not found
```

```
        positions(k,:) = positions(k-1,:);
    end

    % Store time point
    timePoints(k) = (k-1)/frameRate;

    % Display processing every 10 frames
    if mod(k, 10) == 0
        figure(2), imshow(uint8(roi_gray));
        hold on;
        if ~isempty(rows) && ~isempty(cols)
            plot(centroid_x, centroid_y, 'r+', 'MarkerSize', 10);
        end
        hold off;
        title(['Frame ' num2str(k) ' of ' num2str(numFrames)]);
        drawnow;
    end
end

% Determine primary axis of motion (automatically)
x_range = max(positions(:,1)) - min(positions(:,1));
y_range = max(positions(:,2)) - min(positions(:,2));

if x_range >= y_range
    primaryAxis = 1; % x-axis has more movement
    fprintf('Primary motion along X-axis (horizontal)\n');
else
    primaryAxis = 2; % y-axis has more movement
    fprintf('Primary motion along Y-axis (vertical)\n');
end

% Get position data along primary axis
positionData = positions(:, primaryAxis);

% Simple moving average filter without using movmean
windowSize = 5;
smoothedData = positionData;
if length(positionData) > windowSize
    for i = windowSize:length(positionData)
        smoothedData(i) = mean(positionData(i-windowSize+1:i));
    end
end

% Simple detrending without using detrend function
t = (0:length(smoothedData)-1)';
p = polyfit(t, smoothedData, 1);
trend = polyval(p, t);
detrended = smoothedData - trend;

% Plot position vs time
figure(3);
plot(timePoints, positionData, 'b-', timePoints, smoothedData, 'r-');
legend('Raw Position', 'Smoothed Position');
title('Object Position vs Time');
xlabel('Time (s)');
ylabel('Position (pixels)');
grid on;
```

```
    % Calculate amplitude (peak-to-peak)/2
    amplitude = (max(smoothedData) - min(smoothedData)) / 2;

    % Frequency analysis using FFT (doesn't require toolbox)
    if length(detrended) > 10
        % Apply simple windowing (approximate Hamming window)
        N = length(detrended);
        win = 0.54 - 0.46 * cos(2*pi*(0:N-1)'/(N-1));
        windowed = detrended .* win;

        % Compute FFT
        Y = fft(windowed);
        P2 = abs(Y/N);
        P1 = P2(1:floor(N/2)+1);
        P1(2:end-1) = 2*P1(2:end-1);

        % Define frequency domain
        Fs = frameRate;
        f = Fs * (0:(N/2))/N;

        % Plot frequency spectrum
        figure(4);
        plot(f, P1);
        title('Frequency Spectrum');
        xlabel('Frequency (Hz)');
        ylabel('Magnitude');
        grid on;

        % Find peaks in frequency spectrum (simple approach without findpeaks)
        minPeakFreq = 0.5; % Minimum peak frequency to consider (Hz)
        validIndices = find(f > minPeakFreq & f < Fs/2); % Exclude very low and
high frequencies

        if ~isempty(validIndices)
            [maxMag, maxIdx] = max(P1(validIndices));
            dominantFreq = f(validIndices(maxIdx));

            % Display results
            fprintf('\nAnalysis Results:\n');
            fprintf('Dominant Frequency: %.2f Hz\n', dominantFreq);
            fprintf('Amplitude: %.2f pixels\n', amplitude);

            % Convert frequency to RPM
            rpm = dominantFreq * 60;
            fprintf('Rotation Speed: %.2f RPM\n', rpm);

            % Mark the dominant frequency on the plot
            hold on;
            plot(dominantFreq, maxMag, 'ro', 'MarkerSize', 10);
            text(dominantFreq, maxMag, [' ' num2str(dominantFreq, '%.2f') '
Hz'], 'FontSize', 10);
            hold off;
        else
            fprintf('No clear frequency peak detected.\n');
        end
    else
```

```
        fprintf('Not enough data points for frequency analysis.\n');
    end

    % Save the position data to a file for further analysis if needed
    try
        save('motion_data.mat', 'timePoints', 'positionData', 'smoothedData');
        fprintf('Motion data saved to motion_data.mat\n');
    catch
        fprintf('Could not save motion data to file.\n');
    end
end
```

Appendix I: Frequencies of leaf when vortex shedding in induced

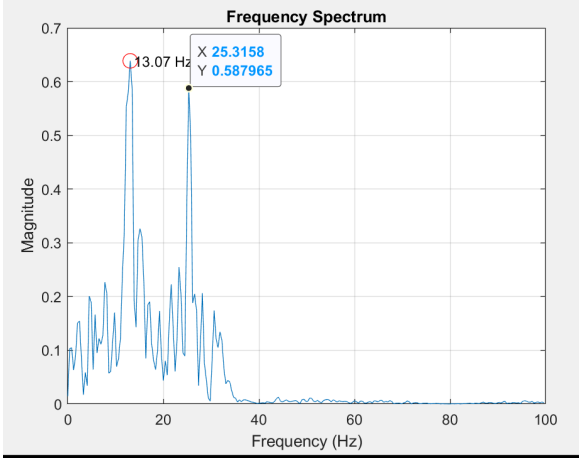

Fig 1: 2.5 MPH (100 RPM) Induced Frequency of 5.58 hz

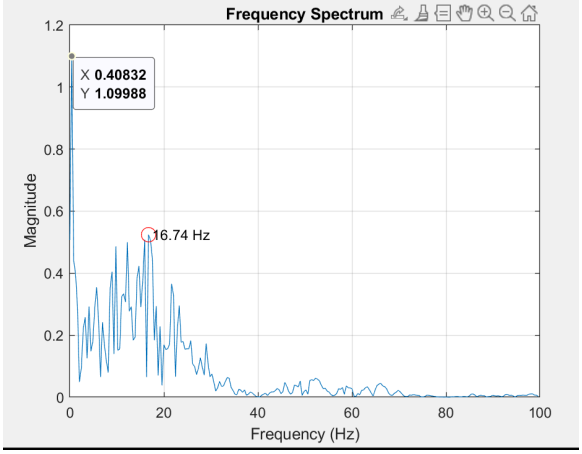

Fig 2: 5 MPH (1500 RPM) Induced Frequency of 11.176 hz

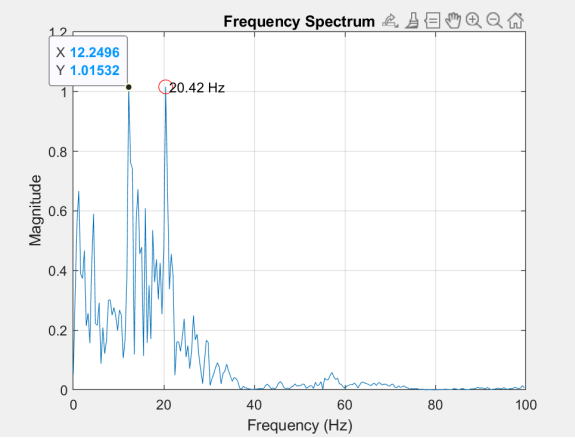

Fig 3: 7 MPH (200 RPM) Induced Frequency of 15.64 hz

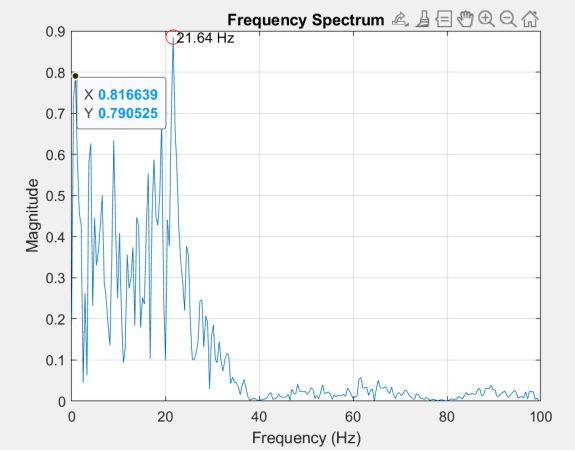

Fig 4: 9 MPH (250 RPM) Induced Frequency of 20.11 hz

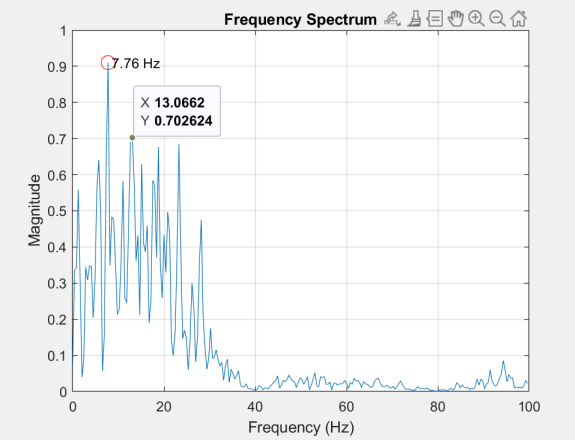

Fig 5: 10 MPH (300 RPM) Induced Frequency of 22.35 hz

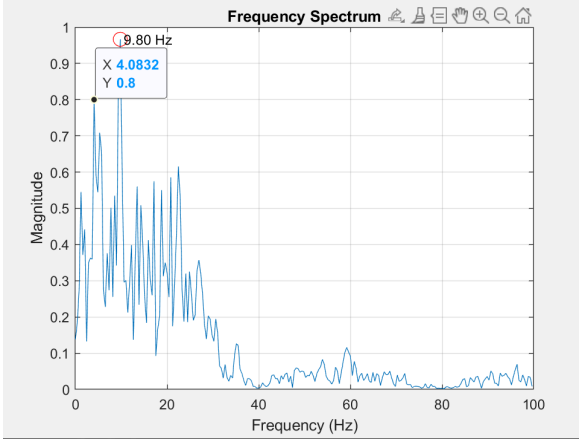

Fig 6: 12 MPH (350 RPM) Induced Frequency of 26.82 hz

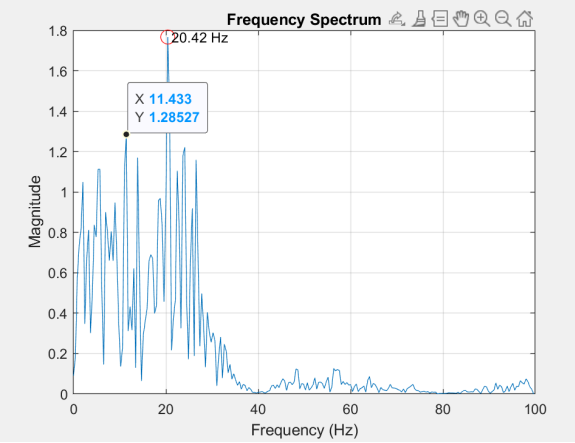

Fig 7: 14 MPH (400 RPM) Induced Frequency of 31.1 hz

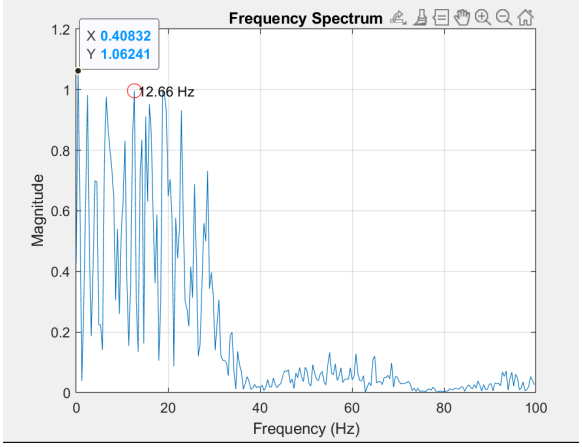

Fig 8: 17 MPH (450 RPM) Induced Frequency of 38 hz

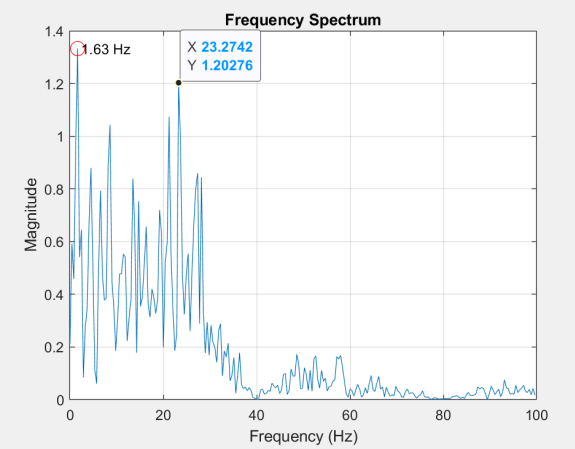

Fig 9: 19 MPH (500 RPM) Induced Frequency of 42.469 hz

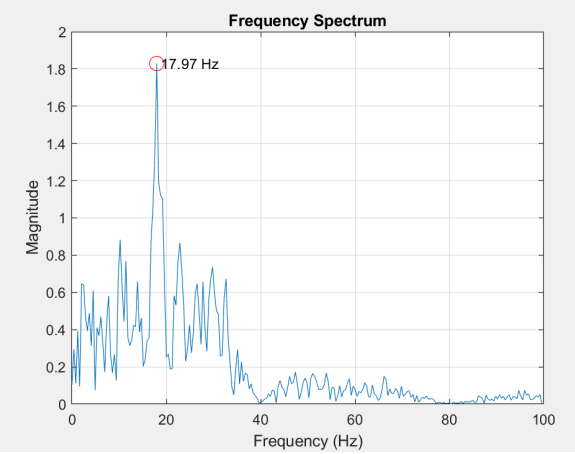

Fig 10: 20.5 MPH (550 RPM) Induced Frequency of 45.82 hz

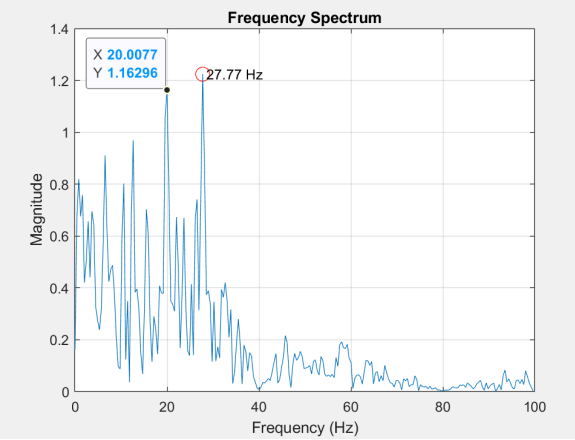

Fig 11: 23 MPH (600 RPM) Induced Frequency of 51.41 hz

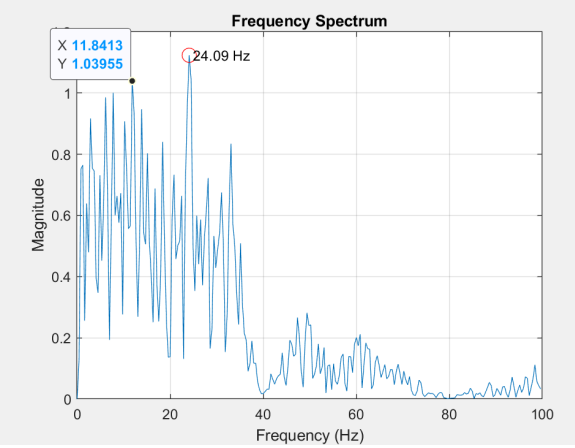

Fig 12: 24.5 MPH (650 RPM) Induced Frequency of 57.76 hz

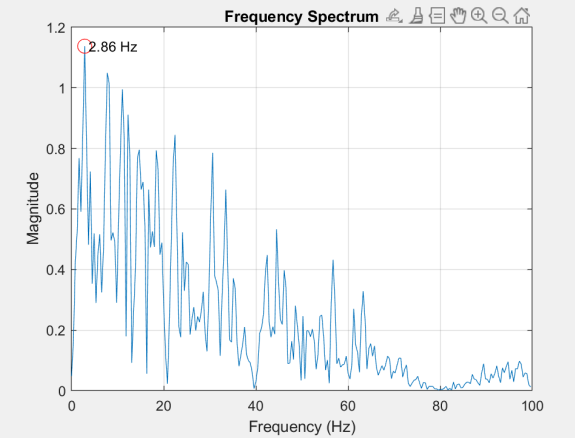

Fig 12: 26.5 MPH (700 RPM) Induced Frequency of 59.23 hz

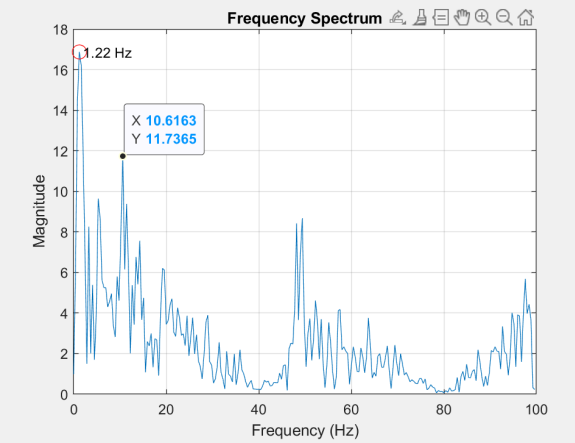

Fig 13: 28 MPH (750 RPM) Induced Frequency of 62.59 hz

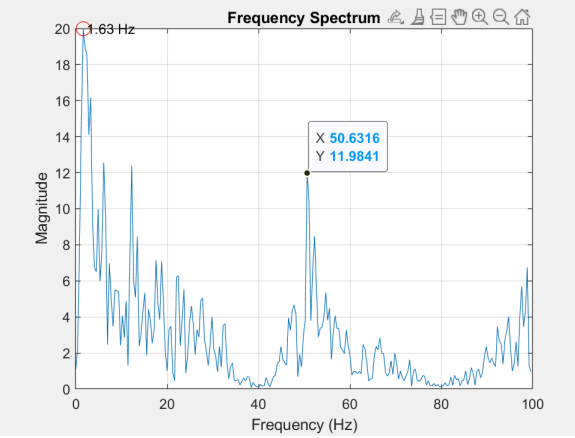

Fig 14: 30 MPH (800 RPM) Induced Frequency of 67.06 hz